Chemical Geology 417 (2015) 184–199

Contents lists available at ScienceDirect

Chemical Geology

journal homepage: www.elsevier.com/locate/chemgeo

A spectrum of disequilibrium melting preserved in lava-hosted, partially melted crustal xenoliths from the Wudalianchi volcanic field, NE China

Lucy E. McGee [a], Claire McLeod [b,1], Jon P. Davidson [c]

[a] Centro de Excelencia en Geotermia de los Andes (CEGA) and Departamento Geología, Universidad de Chile, Santiago, Chile
[b] Department of Earth and Atmospheric Sciences, University of Houston, TX, USA
[c] Department of Earth Sciences, Durham University, UK

ARTICLE INFO

Article history:
Received 10 August 2015
Received in revised form 26 September 2015
Accepted 28 September 2015
Available online 24 October 2015

Keywords:
Anatexis
Crustal xenolith
Disequilibrium melting
Sr-isotopes

ABSTRACT

Disequilibrium melting has been established as a common process occurring during crustal anatexis and thus demonstrates that crustal assimilation is not a closed system. Observations of extreme compositional heterogeneity within partial melts derived from crustal xenoliths have been documented in several recent examples, however, the retention or transfer of elements to and from residues and glasses, and their relative contributions to potential crustal contaminants warrants further investigation. Recent eruptive products of the Huoshaoshan volcano in the Holocene Wudalianchi volcanic field of Northeast China contain crustal xenoliths which preserve a spectrum of partial melting both petrographically and geochemically, thus providing an excellent, natural example of crustal anatexis. Correlations exist between the volume of silicic glass preserved within the xenoliths and bulk rock SiO_2 (70–83 wt.%), Al_2O_3 (8–16 wt.%), glass $^{87}Sr/^{86}Sr$ (0.715–0.908), abundances of elements common in feldspars and micas (Sr, Ba, Rb) and elements common in accessory minerals (Y, Zr, Nb). These correlations are likely associated with the consumption of feldspars and micas and the varying retention of accessory phases during partial melting. The xenoliths which contain greater volumes of silicic glass and residual quartz (interpreted as being the most melted) were found within pahoehoe lava, whilst the least melted xenoliths were found within scoria of the summit cone of Huoshaoshan; thus it is interpreted that the extent of melting is linked to the immersion time in the lava, which we estimate to be on the order of days. However, the least partially melted samples display geochemical evidence in support of melt loss, evidenced by the relatively depleted nature of their whole rock compositions and the larger difference between whole rock and glass. Yet the more melted samples appear to have experienced less melt loss. Thus the extent of melting cannot be linked linearly to the volume of melt loss which occurs. Small-scale (mm) mingling and transfer of material from the enclosing lava to the xenolith are observed, however, modelling of potential contaminant compositions is inconsistent with crustal contamination during lava petrogenesis. It is thus more likely that any crustal contamination in these eruptives is extremely localized within this open magmatic system and most likely occurs at the contact zone between the xenolith and host lava.

1. Introduction

The contamination of mantle-derived magmas by the surrounding continental crust has been recognized as an important petrogenetic process since Bowen (1928) highlighted the likelihood for wallrock assimilation by an ascending magma through the latent heat of fractional crystallisation. Numerous studies of volcanic rocks produced in regions of thickened continental crust have demonstrated that magmatic differentiation occurs in open systems and have established the important role of one or more compositionally distinct crustal components during petrogenesis (e.g. Annen et al., 2006; de Silva, 1989; Hildreth and Moorbath, 1988; Kay et al., 2010). The process of crustal contamination has been investigated and modelled extensively over the past few decades through various combined assimilation–fractional crystallisation (AFC) computations and models (DePaolo, 1981; Grove et al., 1988; Spera and Bohrson, 2001; Taylor, 1980, amongst others). Quantification of the crustal component in open magmatic systems is often challenging as many of the parameters required for modelling are unknown and/or poorly constrained — such as mineral-melt partition coefficients and the geochemical composition of the crustal contaminant.

Additional complication is introduced by limited constraints on the process through which the crust melts in these open systems. Interaction between ascending magma and assimilated wallrock can produce geochemically heterogeneous signatures within a single sample suite, variable petrography and micro- and macro-scale features associated with partial melting and contamination of both end members. One of

E-mail addresses: lucy.e.mcgee@gmail.com, lucymcgee@ing.uchile.cl (L.E. McGee).
[1] Now at: Department of Geology and Environmental Earth Science, Miami University, OH, USA.

http://dx.doi.org/10.1016/j.chemgeo.2015.09.023
0009-2541/

the best-documented examples of these processes is that of the El Joyazo meta-pelitic enclaves hosted in dacite, in southern Spain (Acosta-Vigil et al., 2010, 2012; Cesare, 2000; Cesare et al., 1997). Studies of these partially melted crustal enclaves have evaluated the textural and chemical effects of crustal anatexis through detailed study and analysis of the mineral and glass phases within the enclaves, and have demonstrated the importance of accessory phases to element budgets in crustal-derived partial melts (Acosta-Vigil et al., 2012).

At El Joyazo, crustal anatexis resulted from regional metamorphism rather than the interaction between ascending magma and wallrock(s). Partial melting of wallrock in ascending magma has been documented in several studies, such as the partially fused felsic xenoliths within alkali-olivine basalts from the Northern Cordillera, British Columbia which have either reacted with or contain invasions of the host magma, contain 60–90% glass, relict quartz and feldspar and are highly vesicular (Russell and Hauksdóttir, 2001). Additional examples are xenoliths in basaltic cinder cones of the Mojave Desert of southern California (Knesel and Davidson, 1999), and assimilation of granite at Medicine Lake Volcano (Grove et al., 1988). Another such example is the study of the emplacement of a basalt-andesitic plug into granite country rock in Eastern California investigated by Al-Rawi and Carmichael (1967), where an increase in glass and a decrease in feldspar abundance were observed in the intruding rock near to the contact. This was inferred to be due to preferential melting of feldspar. Natural occurrences of anatexis and experimental studies have sought to determine the behaviour of minerals during crustal partial melting, both in terms of elemental abundances and isotopic compositions (Acosta-Vigil et al., 2012; Ayres and Harris, 1997; Hogan and Sinha, 1991; Knesel and Davidson, 1996; McLeod et al., 2012; Waight and Lesher, 2010; Watson, 1982). These studies highlight the importance of disequilibrium between melt and residuum and demonstrate this process as an inherent feature of crustal anatexis.

The causes of the heterogeneous nature of anatectic melts (i.e. those produced by the breakdown of protolith mineral phases), such as the solubility of individual mineral phases and selective contamination by the melts produced, warrant further investigation of naturally occurring examples in order to evaluate the geochemical budgets of these open magmatic systems. This study reports results from geochemical analyses of a suite of naturally occurring partial melts which have been quenched to glass within their crustal protoliths from the Huoshaoshan volcano in the Wudalianchi volcanic field of Northeast China. These samples therefore preserve the relationship between an anatectic melt and its source. Geochemical analyses complement petrographic observations and record a spectrum of partial melting within the xenolith suite that can be related to the qualitative immersion time of each crustal xenolith within the enclosing basalt.

2. Geological setting

The Wudalianchi volcanic field (48.72° N, 126.12° 88 E) is one of the three Cenozoic potassic volcanic fields that postdate late Mesozoic calc-alkaline volcanism in the western Heilongjiang Province of NE China (Fig. 1). The Wudalianchi field covers an area of *c.* 800 km^2 and consists of fourteen Quaternary volcanoes (Hsu and Chen, 1998; Zou et al., 2003), the most recent of which are Laoheishan and Huoshaoshan (1719–1721 AD). Present theories for the origin of intraplate volcanism in NE China include: the existence of a mantle plume/hotspot (Kuritani et al., 2011), lithospheric thinning/delamination from *c.* 200 km in the Palaeozoic to the present day *c.* 80 km (Wilde et al., 2003), and, contrary to this latter theory, upwelling caused by piling up of stagnant slab (Zou et al., 2008). It is generally understood that the Wudalianchi magmas have an origin in the subcontinental lithospheric mantle, similar to the mantle reservoir of EM I (Zhang et al., 1995; Zou et al., 2003) although recent work has hypothesised an origin at the mantle transition zone with heterogeneity being caused by the input of ancient sediments from the proposed stagnant slab (Kuritani et al., 2013). Phlogopite-bearing garnet peridotites have been inferred as the dominant source rocks with primary magmas generated by small degrees of partial melting at *c.* 80–120 km depth (*c.* 20–45 kbar) at temperatures of *c.* 1068–1100 °C (Zhang et al., 1995; Zou et al., 2003; Wang and Chen, 2005). More recent calculations by Kuritani et al. (2013) from olivine compositions suggest temperatures may have been as high as 1250 °C (assuming crystallisation from a magma containing at least 1.1 wt.% water).

The underlying continental basement of the Wudalianchi volcanic field consists of pre-Permian metasedimentary rocks, Jurassic to Cretaceous volcanic and sedimentary rocks, and late Paleozoic to Jurassic granites (Zhang et al., 1995; Zou et al., 2003). The granites are typically biotite bearing but are noted as being muscovite-bearing in parts (Feng and Whitford-Stark, 1986; Zhang et al., 1995). Overlying the granites are Cretaceous sediments that consist of interbedded muds, shales and sands of lacustrine origin (Feng and Whitford-Stark, 1986). Although xenoliths of granites, schist, sedimentary rocks and volcanic rocks have been found in basaltic products from all three of the Cenozoic potassic volcanic fields in NE China (Zhang et al., 1995), only granitic and sedimentary xenoliths have been found within the Wudalianchi volcanic fields. These granitic and sedimentary lithologies outcrop close (<3 km) to the vents of Laoheishan and Huoshaoshan (Feng and Whitford-Stark, 1986; Fig. 1). Biotite schists and gneiss are known to be basement rock types on a regional scale (Wu et al., 2012).

3. Sample petrography

Six partially melted crustal xenoliths and one sample of the basalt lava from Huoshaoshan form the basis of this work. Unmelted granite xenoliths were also sampled with the hypothesis that these represent the protolith to the partially melted xenoliths. Granite sampled from the same area is briefly described here, as its mineral compositions are used for comparisons with the xenoliths and modelling in the later discussion.

3.1. Lava

The sampled lava consists predominantly of a glassy and fine-grained groundmass consisting of clinopyroxene, feldspar, olivine, glass and Fe–Ti oxides. Olivine, rare augite and rare nepheline are present as phenocryst phases (<10%). Rare quartz xenocrysts (*c.* 4 mm) are present in hand specimen. Previous studies of the potassic volcanism in this area have also reported leucite, sodalite, phlogopite and minor rutile and apatite (Feng and Whitford-Stark, 1986; Hsu and Chen, 1998; Zhang et al., 1995).

3.2. Xenoliths

The xenoliths were sampled from the summit of Huoshaoshan (xenoliths 3a and 3b), and the recent 1719–1721 lava flows (xenoliths 5a, b, c and d). They are characterized by quenched silicic melt, now glass (Figs. 2–3). In hand specimen they display a pumice-like texture (friable) due to the abundant vesicles which range from 0.4 to 3.2 cm. Vesicles appear rounded to sub rounded and occasionally show evidence of preferential orientation. The petrography of the xenoliths is summarized in Fig. 3 and discussed below.

3.2.1. Xenoliths 3a, and b

These xenoliths are hosted in lava that exhibits an a′a-like texture. Xenolith 3a is dominated by vesicles that comprise ~45% of the sample (Fig. 3). The remaining portion of the sample consists of silicic and mafic glass (~12% and 9% respectively, once vesicles are excluded) which can be seen mingling (Fig. 4), polycrystalline and strained quartz, plagioclase feldspar and relict biotite (Fig. 3A). Xenolith 3b is dominated by vesicles (40%) that are on average larger than those in 3a. The remaining crystalline assemblage is composed of polycrystalline and strained quartz, silicic glass (22%), altered plagioclase and rare muscovite (1%).

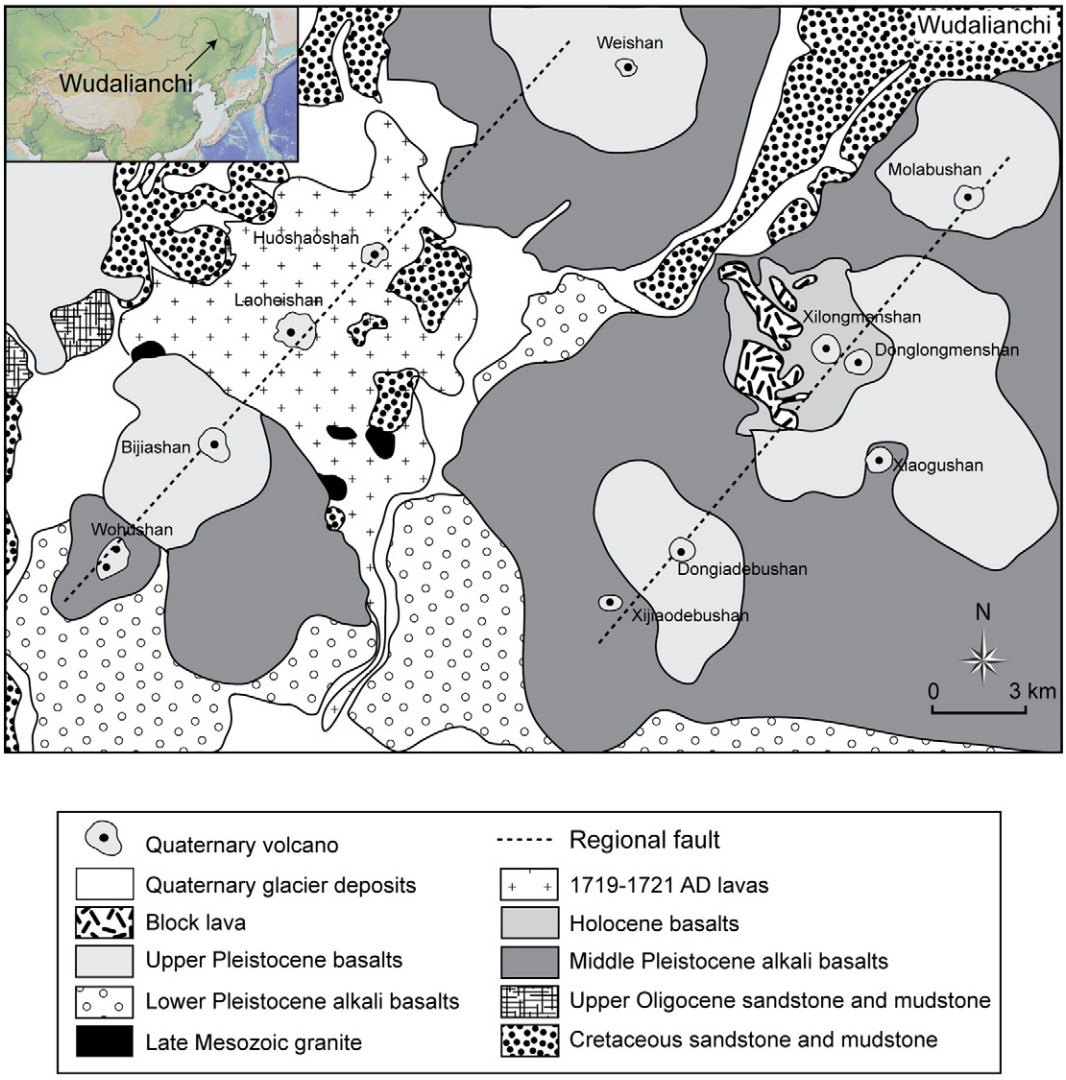

Fig. 1. Geological map of the Wudalianchi region showing the location of the Wudalianchi volcanic field in NE China (inset) and the 14 Quaternary eruption centres including Huoshaoshan and Laoheishan.
Modified from Xiao and Wang (2009).

3.2.2. Xenoliths 5a, b, c, and d

These xenoliths are hosted in pahoehoe-textured lava. They are composed of 65–70% vesicles, and once these are excluded, 55–70% silicic glass (Fig. 3). Micro-scale mingling between melts from the xenoliths and the lava host is clearly seen in the complex mixing zone at the lava–xenolith contact of sample 5b and an olivine crystal appears to have been incorporated into the surrounding vesicles and colourless glass becoming "stranded" (Fig. 4). Quartz is more polycrystalline than strained compared to xenoliths 3a and 3b, and ranges between 25% and 45%.

3.3. Granite

Two samples of unmelted granite were taken from outcrops of the basement close to the historic volcanoes; these samples were collected as they represent a potential protolith to the partially melted xenoliths collected at Huoshaoshan. Their petrography is described here to aid discussion and modelling of the possible protolith in the later discussion. Quartz, microcline, biotite (often altered to chlorite) and plagioclase dominate the mineralogical assemblage (~95%) in addition to rarer orthoclase (<5%), titanite and minor apatite (<1%). Crystals are inequigranular, ranging between 0.5 and 6 mm. Microperthitic textures are often displayed in the alkali feldspar, and some feldspars have broken down to clay.

4. Analytical methods

Samples of the xenoliths were coarse-crushed and any pieces of lava removed so as to ensure only the bulk xenolith was prepared for analysis. Bulk rock powders, mineral separates and glass (cleaned, dried, sieved and picked under the microscope) from the lava, granite and sampled xenoliths were dissolved in HF and HNO_3 using standard dissolution procedures. In preparation for isotopic analyses, sample solutions were passed through standard cation exchange columns. Bulk rock major elements were measured by XRF at the School of Geosciences, University of Edinburgh and errors were <5%. Trace elements were analysed on the X-Series2 ICPMS at the Durham Geochemistry Center (DGC), Durham University, UK following the procedures detailed in Ottley et al. (2003). The errors on reported trace element data range between 1 and 6% with some of the HREE displaying errors up to 10% due

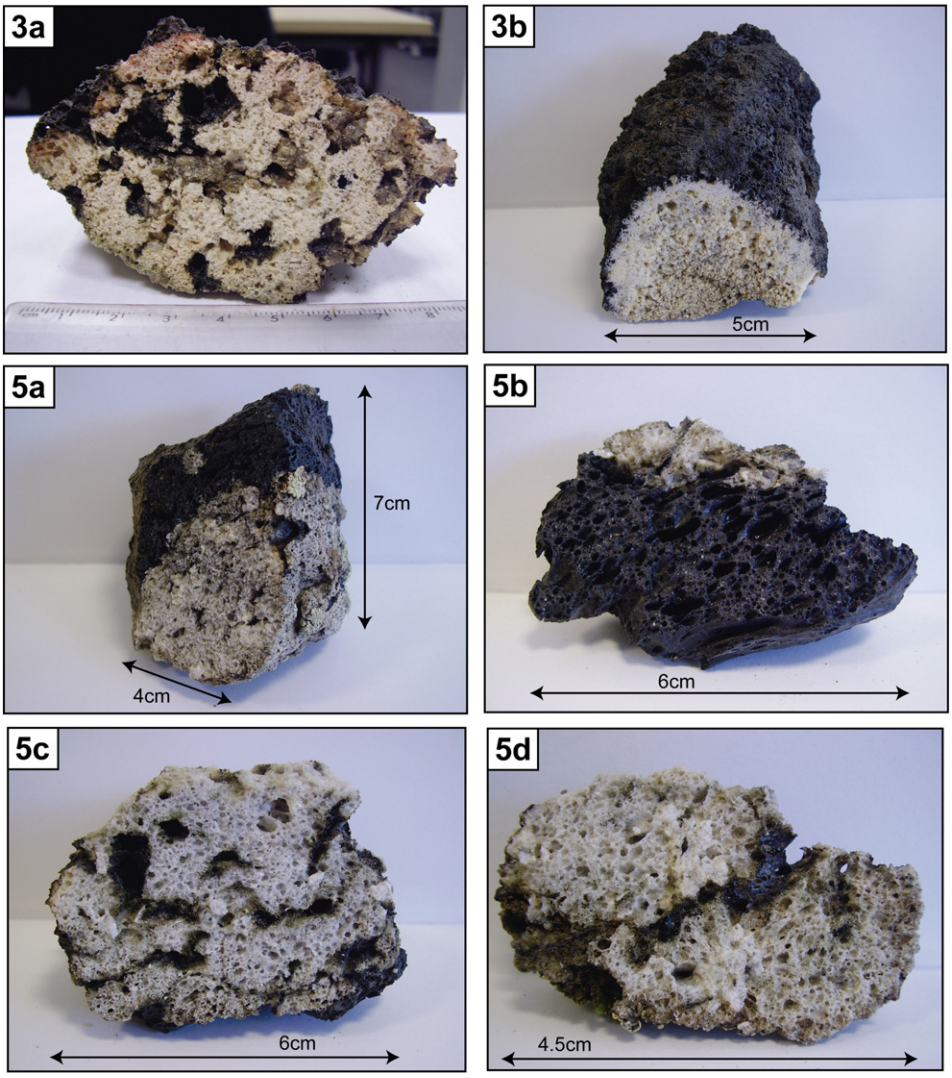

Fig. 2. Hand specimens of partially melted xenoliths from within scoria (3a and 3b) and lava (5a–d), Huoshaoshan volcano, Wudalianchi.

to low concentrations (≤1 ppm). Repeat analyses of international standards were within <5%.

Isotope ratios for Sr and Nd on whole rock powders were determined using a plasma ionisation multicollector mass spectrometer (PIMMS) ThermoElectron Neptune instrument at the DGC. Instrument running conditions and data correction procedures are given in Nowell and Parrish (2001) and Nowell et al. (2003). Reproducibility on the acquired Sr data was tested by repeat measurement of the NBS987 standard which yielded an average $^{87}Sr/^{86}Sr$ of 0.710255 ± 0.000008 (n = 10, 2σ). This is in excellent agreement with values reported by Thirlwall (1991) of 0.710248 ± 0.000023 (n = 247, 2σ). Instrumental mass bias was corrected for using the $^{88}Sr/^{86}Sr$ ratio (the reciprocal of the $^{86}Sr/^{88}Sr$ ratio) and an exponential law. Reproducibility on the acquired Nd data was tested by measuring the J&S standard, a Sm-doped J&S standard and two USGS standards; BHVO-1 and BIR-1. During analysis of the sampled xenoliths average $^{143}Nd/^{144}Nd$ values for the standards were 0.511116 ± 0.000006 (n = 8, 2σ); 0.511121 ± 0.000006 (n = 6, 2σ); 0.512991 ± 0.000010 (n = 3, 2σ) and 0.513098 ± 0.000007 (n = 3, 2σ) respectively. Instrumental mass bias was corrected for by using a $^{146}Nd/^{145}Nd$ value of 2.079143 (equivalent to a $^{146}Nd/^{144}Nd$ value of 0.7219 which is more commonly used) and an exponential law. The $^{146}Nd/^{145}Nd$ value is used because the Nd isotopic compositions of samples are measured on a total REE-cut from the first stage of cation column chemistry and this ratio is the only Ce and Sm free stable Nd isotopic ratio. The use of the $^{146}Nd/^{145}Nd$ however requires a correction for isobaric interferences from Sm on ^{144}, ^{148} and ^{150}Nd. This correction is based on the method given in Nowell and Parrish (2001). The values for the in-house standard are comparable to those reported by Pearson and Nowell (2005) for the long-term reproducibility of this standard: 0.511102 ± 0.000016 (n = 360, 2σ) and 0.511105 ± 0.000017 (n = 202, 2σ).

Strontium isotopes for glass and mineral separates were analysed by thermal ionisation mass spectrometry (TIMS) at the DGC. Running conditions of the Thermo-Finnigan Triton TIMS system (and data corrections) are given in Font et al. (2008). Picked glass and mineral separates were dissolved in ultra-pure acids (HNO_3 and HF) and the Sr fraction was then separated using the micro-Sr column procedure given in Charlier et al. (2006). $^{87}Sr/^{86}Sr$ and $^{84}Sr/^{86}Sr$ ratios were corrected for mass fractionation using an exponential law and a $^{86}Sr/^{88}Sr$ ratio of 0.1194. During this study, 24 analyses for the $^{87}Sr/^{86}Sr$ composition of the international standard NBS 987 yielded an average $^{87}Sr/^{86}Sr$ of 0.710269 ± 0.000010 (2σ) which is in excellent agreement with the values reported by Thirlwall (1991) of 0.710248 ± 0.000023 (n = 247, 2σ). All sample data is presented in Tables 1–3.

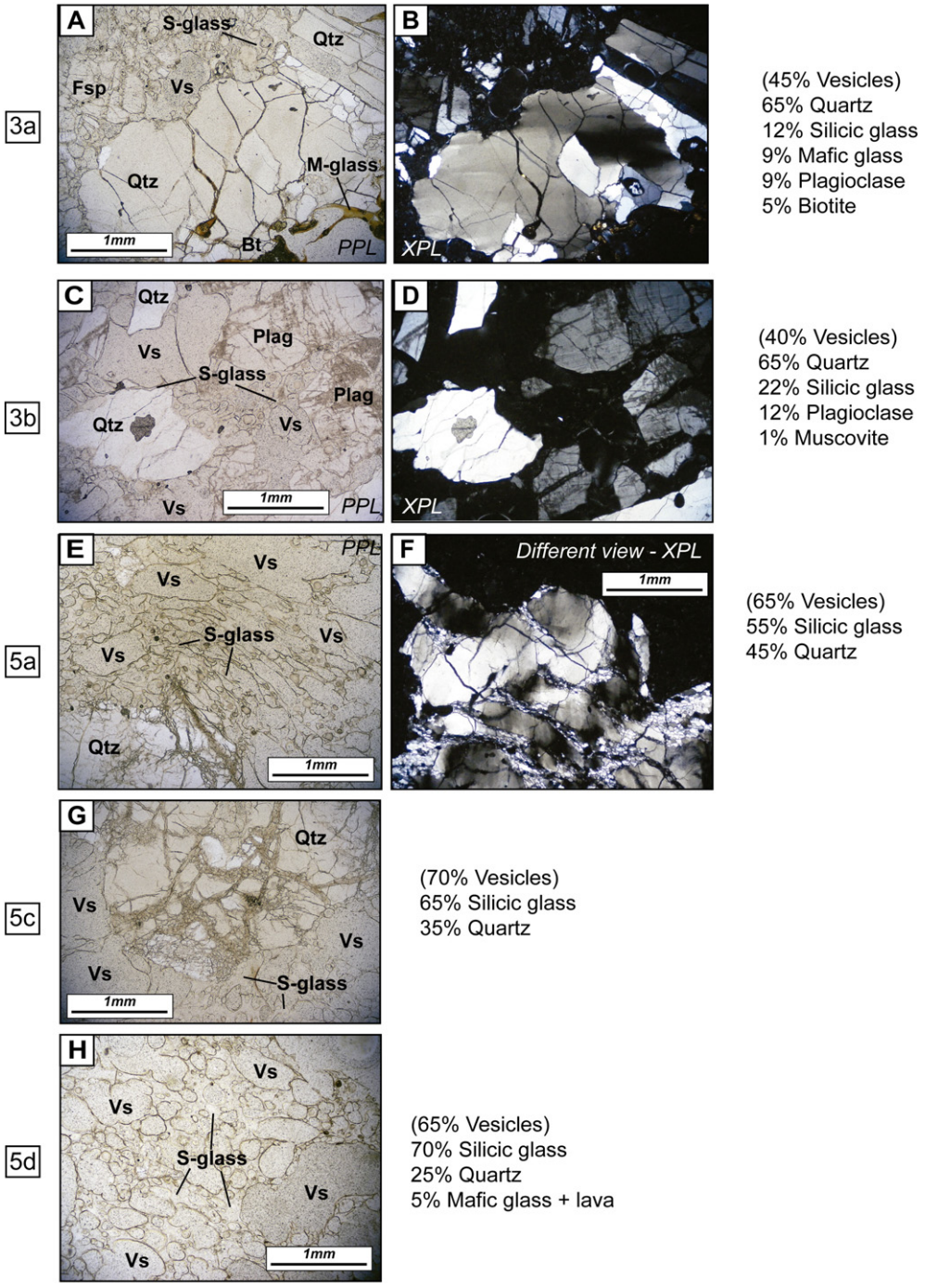

Fig. 3. Thin section photomicrographs of the studied xenoliths at Huoshaoshan. Field of view in all photographs is approximately 3 mm. Approximate percentages of minerals and glass are given against each xenolith (note that percentages are given of the whole rock discounting vesicles). The xenoliths are very heterogeneous texturally, and representative photographs are shown here to demonstrate the main features of each one: undulose extinction of quartz and the presence of mafic glass (M-glass) in 3a, the presence of plagioclase in 3b, the abundance of silicic glass (S-glass), more elongate vesicles (Vs) and polycrystalline quartz in 5a, 5c and 5d. XPL images are not shown for 5c and 5d as due to the abundance of vesicles and S-glass in these xenoliths their features are best observed in PPL.

5. Results

The focus of this work is on the composition of the xenoliths, their constituent minerals, preserved glass and the bulk rock and mineral compositions (feldspar, biotite and titanite) of the collected granite sample. Results are presented alongside complementary data from local crustal basement outcrops in the area from previously published work: monzogranite, biotite (Bt-) gneiss and biotite (Bt-) schist after Wu et al. (2012). These comparisons are principally used to aid the later discussion but are shown here for completeness.

5.1. Whole rock chemistry

5.1.1. Major and trace elements

The most striking feature within the major elements of the xenolith suite is the strong negative correlation in total alkalis (ranging from 6–12 wt.%, Fig. 5A) and Al_2O_3 (9–17 wt.%, Fig. 5B) with increasing SiO_2, and extremely low values of FeO and CaO (Fig. 5C and D, Table 1). The sampled granite, Bt-schist and Bt-gneiss have higher concentrations of FeO and CaO than the xenoliths, and lower total alkalis. In Al_2O_3 content, the xenoliths plot close to the granite and Bt-schist, with the Bt-gneiss

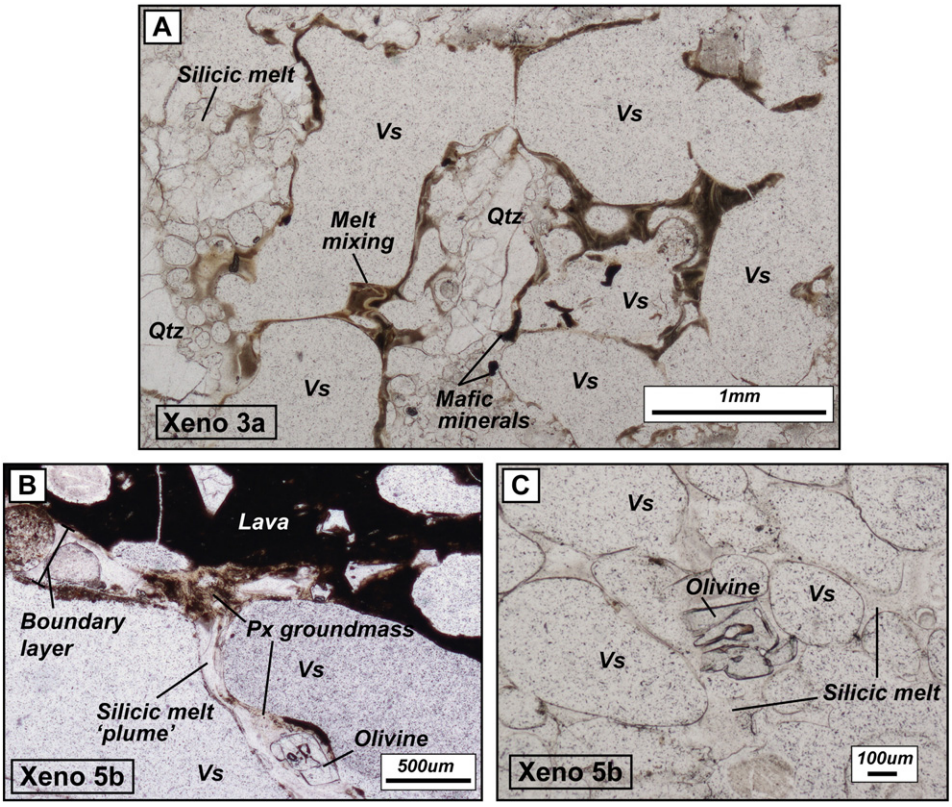

Fig. 4. Petrographic evidence of the exchange of material between partially melted crustal xenoliths and enclosing lava. A. Xenolith 3a: Colourless and brown glasses are complexly intermingled, and may be indicative of either incomplete mixing post breakdown of a mafic mineral phase such as biotite, or infiltration and incomplete dissolution of lava within the xenolith. B. Lava–xenolith contact in sample 5b showing a complex mixing zone between the colourless and brown glass, and the transfer of an olivine crystal into the xenolith, and C. "stranded" olivine crystal within colourless melt pockets and vesicles of partially melted xenolith 5b. The olivine crystal is assumed to have been transferred from the enclosing basaltic magma to the xenolith when the two materials were partially molten and in contact, indicating micro-scale interaction. Vs = vesicles, Qtz = quartz, Px = pyroxene.

displaying much higher values (*c.* 20 wt.%). The host lava is potassic in nature and strongly alkalic (*c.* 5 wt.% K_2O; Zou et al., 2003; Fig. 5A) and can be classified as a phono-tephrite (Le Maitre, 2002). The lava data displays a strong negative correlation in CaO *vs.* SiO_2, and a positive correlation in Al_2O_3 *vs.* SiO_2.

Selected trace element analyses are shown in Fig. 6 (see Table 1 for all analyses). In general, the xenoliths display heterogeneity within the trace elements, for example ranging between 2 and 36 ppm in Ce (Fig. 6C). Xenoliths 3a and 3b cluster together at higher Sr (58–75 ppm; Fig. 6A) and lower Th (1 ppm; Fig. 6E) and Y (4 ppm; Fig. 6G). Xenoliths 5a, 5b and 5d show the reverse of this: 12–30 ppm, 10–18 ppm and 19–43 ppm in Sr, Th and Y respectively. In comparison with other whole rock compositions, the xenoliths have similar trace element compositions to the sampled granite (Fig. 6D, F and H), although the granite displays much higher Sr (up to 659 ppm; Fig. 6B). The lava displays very high Sr (1480 ppm; Fig. 6B), Ba (1600 ppm) and Zr (530 ppm; Table 1), and in general higher trace element contents than the granite and xenoliths, with the exception of Th (Fig. 6F).

The Bt-schist and Bt-gneiss (Wu et al., 2012) have similar patterns, with the only difference being in the degree of the Sr depletion. The granite (this study) displays a more depleted trend (almost an order of magnitude different to the Bt-gneiss and Bt-schist, when normalized to primitive mantle) with a notable peak at Sr and depletion at Zr. The monzogranite is similar to the Bt-schist and gneiss, but has higher incompatible element contents. All four basement rock types exhibit Nb–Ta depletion relative to primitive mantle (Fig. 7A). Xenoliths 3a and 3b are plotted separately to xenoliths 5a, b and 5d on multi-element plots as they display similar characteristics within their groups, but are notably distinct from each other (Fig. 7B and 7C). The group 3 xenoliths are more variable in trace element content, for example showing contrasting peaks/depletions in Sr, Sm, Eu and Yb, but are characterized by a generally steep pattern from the incompatible to compatible elements (Fig. 7B). The group 5 xenoliths, however, are more similar, and are less depleted in the more compatible elements. All group 5 xenoliths display pronounced depletions in Ba, Sr and Eu, and peaks at U, Th and Ta, and higher concentrations of HREE (Fig. 7C). Within this group, 5d has higher abundances of HREE, Zr (110 ppm) and Hf (3.6 ppm) compared to xenoliths 5a (40 ppm and 1.47 ppm in Zr and Hf respectively) and 5b (30 ppm and 1.11 ppm in Zr and Hf respectively).

5.1.2. Sr–Nd isotopes

The sampled xenoliths show significant diversity with respect to $^{87}Sr/^{86}Sr$, ranging from 0.71327 to 0.76403 (Fig. 8A). These signatures are notably more radiogenic than previously reported compositions for the local basement in the region: 0.7052–0.7145 (Zhang et al., 1995). Xenoliths 3a and 3b and xenolith 5d display $^{143}Nd/^{144}Nd$ values of 0.51275–0.51289. The host lava displays relatively restricted $^{87}Sr/^{86}Sr$ (0.70505–0.70538) over $^{143}Nd/^{144}Nd$ from 0.51238–0.51245 (Zhang et al., 1995; Zou et al., 2003). The sampled granite exhibits lower $^{87}Sr/^{86}Sr$ compared to the xenolith suite (0.7053) but similar $^{143}Nd/^{144}Nd$ to xenolith 3a (0.51273).

5.2. Mineral and glass chemistry

5.2.1. Trace elements

In general, the glasses contained within the xenoliths are lower in trace element abundances than the bulk xenoliths (Figs. 6 and 7). With respect to the incompatible elements, Th and Y define a striking

Table 1
Whole rock major and trace element and Sr–Nd isotopic analysis for the lava, two samples of basement granite, and the xenolith suite. Note that Sr–Nd isotopes were not obtained for sample 5b due to a limited quantity of sample powder and abundance of lava infiltration (see Fig. 2). Errors on isotopes are 1 SE.

	Whole rock							
	Lava	Granite 1	Granite 2	Xenolith 3a	Xenolith 3b	Xenolith 5a	Xenolith 5c	Xenolith 5d
SiO_2	51.8	68.2	69.8	69.8	74.4	74.6	72.4	82.9
TiO_2	3.9	0.4	0.5	—	0.1	0.1	0.1	0.1
Al_2O_3	2.2	15.3	14.7	16.5	13.9	12.7	14.3	8.6
FeO	14.5	2.3	2.6	0.4	0.5	1.2	0.9	0.7
MgO	8.4	1.3	1.4	0.2	0.1	0.2	0.1	0.2
CaO	0.1	2.5	2.1	0.3	1	0.2	0.1	0.1
Na_2O	6.9	4.5	4.2	4.6	4.1	4.5	4.2	3
K2O	6.8	3.2	3.4	7.2	5	4.6	6.8	3.4
MnO	5.1	–	–	–	–	0.1	–	0.1
P_2O_5	1.1	0.2	0.2	–	–	–	–	–
LOI	–	1.7	1	1.2	0.6	1.3	1.1	0.7
Total	100.8	99.5	99.9	100.2	99.6	99.5	100	99.7
$Na_2O + K_2O$	13.7	7.7	7.6	11.8	9.1	9.1	11.0	6.4
K	56,660	26,660	28,330	60,000	41,660	38,330	56,660	28,330
Ti	23,353	2395	2994	—	599	599	599	599
Sc	13	5	5	2	2	3	3	3
V	119	42	51	2	3	5	2	2
Cr	187	37	40	2	2	4	3	2
Co	31	7	6	1	1	1	1	1
Ni	180	21	21	2	—	2	2	1
Cu	35.1	10	1.9	5.4	3.8	2.7	13.9	2.7
Zn	128	39	27	11	11	66	22	27
Ga	23.5	19.2	18	24.7	18.1	22.7	26	15.8
Rb	113.2	73.1	65.4	137.6	111.5	155.8	214.1	124.5
Sr	1480	659	564	58	75	30	21	12
Y	21.9	6	9.1	4.4	3.9	27.8	19.3	42.5
Zr	524	35	35	12	11	42	26	107
Nb	79.05	3.79	6.31	1.18	4.45	9.86	10.13	31.51
Cs	0.89	1.55	3.54	1.16	0.69	1.89	2.09	1.36
Ba	1637	700	760	112	102	46	26	15
La	81.1	13.1	16.1	4.4	2	12.6	3.7	5.4
Ce	152.8	26.2	33.5	9.7	3.7	36.2	11	19.1
Pr	18.52	3.07	5.15	1.29	0.45	5.02	1.61	2.75
Nd	68.6	11.2	20	4.6	1.7	19.1	6.6	11.8
Sm	10.6	1.6	3.3	0.8	0.2	5	2.1	4.7
Eu	2.94	0.56	0.74	0.11	0.44	0.38	0.17	0.33
Gd	7.14	1.25	2.36	0.81	0.43	5.23	3.09	6.68
Tb	0.9	0.19	0.33	0.13	0.08	0.89	0.56	1.28
Dy	4.4	1	1.7	0.8	0.5	5	3.2	7.8
Ho	0.74	0.18	0.33	0.14	0.11	0.91	0.59	1.54
Er	1.58	0.48	0.79	0.36	0.34	2.18	1.43	3.85
Tm	0.22	0.08	0.13	0.05	0.05	0.32	0.21	0.58
Yb	1.22	0.53	0.79	0.3	0.42	1.78	1.18	3.19
Lu	0.17	0.08	0.12	0.04	0.07	0.25	0.16	0.41
Hf	11.42	1.17	1.28	0.36	0.41	1.47	1.11	3.57
Ta	3.67	0.28	0.5	0.12	0.55	0.97	0.7	1.71
Pb	14.2	23.5	9.6	11.6	29.9	14.2	65.9	515.9
Th	6.45	3.87	9.93	1.48	1.2	9.93	14.63	17.86
U	1.38	1.29	1.31	0.3	1.49	2.42	2	5.94
$^{87}Sr/^{86}Sr$	0.705411 ± 5	0.705200 ± 3	0.705402 ± 5	0.716864 ± 6	0.713273 ± 5	0.737135 ± 6		0.760430 ± 10
$^{143}Nd/^{144}Nd$	0.512395 ± 3	0.512747 ± 4	0.512724 ± 3	0.512752 ± 9	0.512800 ± 8	0.512795 ± 3		0.512891 ± 5

Dashes denote values at or close to 0.

positive correlation with Rb from glass 3a to glass 5a (Fig. 6E and 6G). For Sr (Fig. 6A) and Ba (Table 1), the glasses fall within a similar range as the bulk xenoliths, although glass 5a is notably more depleted in these elements compared with glasses 3a and 3b (Fig. 7F). The two feldspar analyses – 3a and 3b from their respective xenoliths – show a wide range in values, with feldspar 3b generally displaying higher values than 3b, and are more variable than the values of the feldspars from the sampled granite. When normalized to the granite feldspars (Fig. 7G), they are demonstrably more enriched in Nb and HREE (in xenolith 3b) and notably more depleted in Ba, Th, Sr, Eu.

Multi-element patterns of the xenolith glasses and feldspars highlight an interesting feature: glasses contained within xenoliths 3a and 3b have a similar pattern to the feldspars sampled from these xenoliths, whereas the glass contained within xenolith 5a displays a pattern almost identical to that of the bulk xenolith, although consistently less by an order of magnitude. No residual feldspar was observed in this xenolith (see petrography section).

5.2.2. Sr isotopes

Sr isotopic ratios for glasses 3a and 3b and feldspar 3a are similar to those of their host xenoliths, however glass 5a displays extreme values ranging up to 0.90868 (Fig. 8B and Table 2). All bulk xenolith and glass values form a positive correlation with the Rb/Sr ratio. It is noted that although the Sr isotopic ratio for the feldspar 3a is similar to the feldspar from the sampled granite, the Rb/Sr ratio is different: 2.1 in the xenolith feldspar compared to 0.03 in the granite feldspar (Fig. 7G).

Table 2
Trace element analyses of the individual components in this study: xenolith glasses for samples 3a, 3b and 5a, feldspars contained in xenoliths 3a and 3b (not present in xenolith 5a) and minerals from the granite, used in the discussion and Figs. 6–8. The final column shows the possible 'residue' of the xenoliths, when the glass compositions are simply subtracted from the whole rock compositions.

	Mineral and glass separates											
	Xenolith glasses			Xenolith feldspars			Granite minerals				Calculated 'residue'	
	Glass_3a	Glass(i)3b	Glass(ii)3b	Glass 5a	Fsp Xeno 3a	Fsp Xeno 3b	Titanite	Fsp 1	Fsp 2	Biotite	Glass 3a	Glass 3b	Glass 5a
Ti	–	178.95	246.27	60.85	–	123.50	32.12	–	–	2.09	–	419.85	537.95
Sc	–	–	–	–	–	–	1.90	–	–	20.60	2.00	2.00	3.00
V	–	–	–	–	–	–	812.00	–	–	321.00	2.00	3.00	5.00
Cr	–	–	–	–	–	–	170.80	–	–	304.90	1.70	2.20	4.10
Co	–	–	–	–	–	–	0.30	–	–	53.30	1.00	1.00	1.00
Ni	–	–	–	–	–	–	128.70	29.80	–	167.60	2.00	–	2.00
Cu	1.00	1.00	1.00	2.00	–	1.00	91.00	7.00	9.00	26.00	4.90	3.22	0.59
Zn	–	–	–	–	–	–	247.95	–	–	106.96	11.00	11.00	66.00
Ga	30.20	18.80	19.50	31.80	30.70	28.80	36.50	23.30	23.80	43.40	−5.23	−0.84	−8.82
Rb	156.12	174.53	184.18	220.62	148.49	34.92	3.86	37.22	70.65	245.88	−18.12	−63.53	−64.62
Sr	75.17	76.26	69.31	7.50	70.08	145.38	204.25	1133.00	1136.31	216.08	−17.17	−1.30	22.50
Y	0.61	2.71	3.18	7.68	0.52	1.72	1317.25	0.47	0.77	16.02	3.39	1.29	20.32
Zr	–	2.84	3.33	6.78	–	0.36	474.18	–	0.26	158.60	10.00	7.16	33.22
Nb	0.11	2.69	3.57	3.30	0.17	1.71	830.84	0.07	0.17	8.56	1.07	1.76	6.56
Cs	1.15	0.86	0.91	2.31	1.30	0.12	0.27	1.28	1.76	13.18	0.05	−0.16	−0.41
Ba	140.44	144.40	135.93	1.45	159.47	8.00	23.78	373.17	571.73	394.58	−27.94	−42.53	44.14
La	1.96	1.68	1.73	1.95	1.11	1.71	1696.86	8.02	8.68	34.09	2.39	0.29	10.64
Ce	3.12	2.88	2.78	5.72	1.89	2.51	4934.43	9.64	10.57	52.03	6.62	0.78	30.51
Pr	0.32	0.35	0.33	0.84	0.22	0.28	689.26	0.85	0.98	5.34	0.97	0.10	4.18
Nd	0.93	1.19	1.07	3.11	0.63	0.88	2892.26	2.44	2.97	18.50	3.63	0.53	15.99
Sm	0.07	0.22	0.23	0.89	0.03	0.12	490.67	0.25	0.32	3.18	0.72	−0.06	4.09
Eu	0.03	0.44	0.46	0.06	0.03	0.56	96.51	0.53	0.48	1.04	0.08	–	0.32
Gd	0.10	0.32	0.33	1.07	0.07	0.16	370.83	0.16	0.23	3.09	0.71	0.11	4.16
Tb	0.01	0.05	0.06	0.20	0.01	0.03	48.03	0.01	0.02	0.44	0.12	0.03	0.69
Dy	0.08	0.36	0.41	1.22	0.06	0.21	248.38	0.07	0.13	2.48	0.67	0.12	3.81
Ho	0.02	0.07	0.08	0.23	0.01	0.05	45.84	0.01	0.02	0.50	0.12	0.04	0.68
Er	0.01	0.19	0.23	0.56	0.01	0.11	116.45	–	0.03	1.35	0.35	0.15	1.62
Tm	–	0.03	0.04	0.08	–	0.02	17.89	–	–	0.22	0.05	0.02	0.24
Yb	0.03	0.24	0.28	0.52	0.03	0.16	111.11	0.03	0.06	1.53	0.27	0.18	1.26
Lu	–	0.04	0.04	0.07	–	0.02	16.23	–	–	0.27	0.04	0.03	0.18
Hf	–	0.17	0.20	0.35	–	0.05	35.31	0.00	0.01	5.54	0.35	0.23	1.12
Ta	–	0.26	0.39	0.53	–	0.15	85.77	0.02	0.01	0.19	0.10	0.34	9.57
Pb	14.04	46.09	44.64	9.88	10.84	26.89	70.39	23.46	22.19	42.99	−2.04	−16.09	4.12
Th	0.21	0.82	1.30	2.91	0.18	0.43	453.39	0.60	0.67	7.10	0.79	0.18	7.09
U	0.08	0.79	1.16	0.45	0.09	0.60	120.18	0.32	0.41	4.45	0.22	0.71	1.95

Dashes denote values at or close to 0.

6. Discussion

Combining the petrographic observations with the chemistry of the bulk rock, glass and mineral phases of the sampled xenoliths highlights several important features associated with crustal partial-melting at Huoshaoshan. First, the disappearance of mineral phases (feldspar and mica), increase in abundance of vesicles and increase in proportion of silicic melt throughout the xenolith suite from 3a to 5d appear to record a spectrum of partial melting (Fig. 3). This corresponds to the bulk rock geochemical signatures (such as the increase in SiO_2 and decrease in Al_2O_3 from xenolith 3a to 5d, Fig. 5) and the complementary glass data of the xenoliths (such as the decrease in Sr and increase in Rb from 3a to 5d, Fig. 6).

Second, the xenoliths form two distinct geochemical groups: xenoliths 3a and 3b: group 3 (Fig. 7B) and xenoliths 5a, 5b and 5d: group 5 (Fig. 7C). Bulk rock analyses of group 3 are more enriched in elements associated with feldspars (Ba, Sr, Eu). The complementary glass data for group 3 is similar to that of the analysed feldspars (Fig. 7D and 7E). Bulk rock analyses of group 5 however are more enriched in elements typically associated with accessory phases (Y, Th, Ce, Fig. 6), although the composition of glass 5a is more enriched than glasses 3a and 3b. The multi-element pattern of glass 5a follows that of the bulk xenolith, and both bulk and glass patterns show large depletions in elements with affinities to feldspars (Sr, Ba and Eu, Fig. 7F). All bulk xenoliths and glasses display negative anomalies in Zr (Fig. 7). With respect to Sr-isotopes, bulk xenoliths exhibit $^{87}Sr/^{86}Sr$ ratios which are

Table 3
Sr isotopic analyses of xenolith glasses 3a, 3b and 5a, the feldspar in xenolith 3a, and feldspar and biotite from the granite sample. Various digestions were made and run for each xenolith glass. Errors on isotopes are 1 SE. Note that larger errors are noted for digestions 3–5 of glass 5a due to lower voltage beams (<1 V).

87Sr/86Sr						
	Xenolith glasses			Xenolith fsp	Granite minerals	
Digestion	Glass 3a	Glass 3b	Glass 5a	Feldspar 3a	Feldspar	Biotite
1	0.715504 ± 8	0.723799 ± 7	0.908683 ± 9	0.720383 ± 22	0.704984 ± 3	0.713843 ± 46
2	0.716399 ± 4	0.721010 ± 12	0.904507 ± 11	0.719389 ± 6	0.704565 ± 3	0.714773 ± 3
3	0.714819 ± 7	0.722060 ± 5	0.893833 ± 36		0.704482 ± 4	0.714356 ± 6
4	0.717460 ± 6	0.723057 ± 9	0.836298 ± 24		0.704721 ± 5	
5	0.717385 ± 5		0.773997 ± 81			

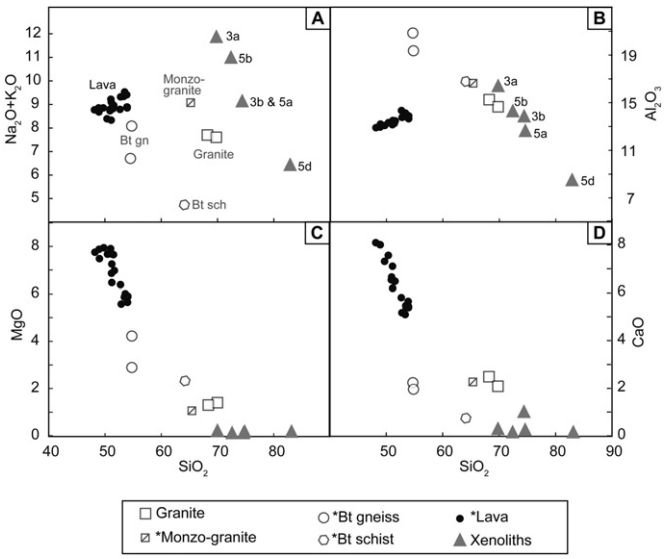

Fig. 5. Bulk rock major element compositions of the Wudalianchi lavas (from Feng and Whitford-Stark, 1986; Zhang et al., 1995; Zou et al., 2003), the partially melted xenoliths 3a, 3b, 5a–d, and several basement rock types. The two granite analyses are from this study, and the monzo-granite, biotite gneiss 'Bt-gneiss' and biotite schist 'Bt schist' are from Wu et al. (2012). Stars in the legend denote literature data. All data are in weight %.

significantly higher than the known granitic or sedimentary local basement rocks. For glasses 3a and 3b, their $^{87}Sr/^{86}Sr$ compositions are similar to those of their host xenolith. For glass 5a, $^{87}Sr/^{86}Sr$ ratios are significantly higher (Fig. 8).

Third, by comparing the bulk chemical signatures of the xenoliths to their respective glasses it is clear that there is a missing component. This is exemplified by the multi-element pattern for xenolith 5a where the glass composition is an order of magnitude lower than that of the whole rock, yet petrographic observations show that the only other phase present is quartz (Fig. 7F; see petrography section). The examples in Fig. 4 show interaction between xenolith derived melt with the enclosing lava. This is a potential mechanism through which material has been lost. However, to assess this as a potential process, the following points need to be addressed: first: what protolith(s) the xenoliths came from, second: the process of melting of the xenoliths (i.e. crustal anatexis) and how the various compositions observed in the xenolith suite can be explained with respect to the ascertained protolith(s), and third: what is the potential for crustal contamination of the surrounding magma and by the 'missing component'.

6.1. The nature of the protolith

Petrographic observations and bulk rock chemistry demonstrate that the group 3 and group 5 xenoliths have distinct residual mineralogy and compositions. This could suggest two things: 1) that the two xenolith groups have distinct protoliths, or 2) the two groups have experienced different degrees of crustal anatexis *en route* to the surface. Evidence supporting the former is the obvious clustering of groups 3 and 5 xenoliths in the bulk rock composition of elements such as Th and Y (Fig. 6), and the fact that they are from different parts of the eruptive sequence, group 3 being from the summit and enclosed in a′a lava, and group 5 being from lava flows and enclosed in pahoehoe lava. However, linear trends in bulk rock xenolith chemistry with respect to SiO_2 *vs.* total alkalis (Fig. 5A), Al_2O_3 (Fig. 5B), $^{87}Sr/^{86}Sr$ *vs.* Rb/Sr (Fig. 8B) and the linear trends in glass chemistry with respect to trace elements (Fig. 6) suggest that the xenoliths are related to a single protolith. If this is the case, either the protolith was mineralogically heterogeneous, or – as suggested above – the two groups experienced different degrees of partial melting during crustal anatexis. This will be discussed in the following section.

As previously mentioned, several basement rock types have been recognized locally and regionally: granites, both biotite and muscovite bearing varieties, or possibly a single granitic lithology that is mineralogically heterogeneous, and sedimentary rocks: mudstone and sandstone, outcrop within the volcanic field itself (Feng and Whitford-Stark, 1986; Xiao and Wang, 2009, see Fig. 1). Additionally, Wu et al. (2012) described various supracrustal igneous and metamorphic rocks in the Heilongjiang region, including biotite schist, biotite–plagioclase gneiss and monzogranites (shown in Figs. 5–7).

Petrographic observations (petrography section and Figs. 3–4) document evidence of the xenoliths' protolith. The residual mineralogy is crystalline, which is an argument against a sedimentary protolith such as the mudstones observed in the area. The presence of colourless and brown glass is evidence of melting of both silicic and mafic mineral phases, along with residual mafic minerals observed in xenolith 3a. Feldspars are observed in xenoliths 3a and 3b, and plagioclase twinning is observed in xenolith 3b. All xenoliths contain quartz, which is often strained, displaying undulose extinction and in group 5 is commonly polycrystalline. This is indicative of a protolith that contained quartz which had experienced stress significant enough to distort the crystal lattice, thus, could imply a metamorphic protolith. These patches of quartz are present either in large (up to 4 mm) areas, or as small elongate laths. This is distinct from the granophyric textures preserved in the xenoliths in the study by Grove et al. (1988), which led to the conclusion that the protolith was granitic.

Another diagnostic feature of the xenolith suite is the ubiquitous presence of vesicles (ranging from 40 to 70%, Fig. 3). This is indicative of either the input of fluids during the transport to the surface, or the presence of a greater abundance of hydrous minerals than is inferred from the residual mineralogy. The former scenario is unlikely as it would imply that the enclosing lava would also be affected, and no visual evidence from hand specimens can be shown to support this e.g. alteration. If the latter scenario – the abundance of hydrous minerals – is correct, this lends further evidence to a protolith distinct from the granite found outcropping near the historic volcanoes, either with a greater abundance of biotite and muscovite, or a metamorphic protolith containing mica(s). The latter could be an explanation for the observed elongation of the vesicles that are particularly pronounced in group 5 xenoliths, and would also explain the 'laths' of quartz observed in some parts that could represent the more resistant residual bands of schistose or gneissic foliations.

The protolith to the partially melted Huoshaoshan xenoliths must therefore have contained abundant quartz, feldspar, hydrous minerals such as biotite (observed) and possibly muscovite (1% muscovite observed in xenolith 3b). The protolith is also likely to have contained accessory phases such as titanite, zircon and/or monazite in order to account for the relatively high abundances of Y, Th, REE and Ta within the group 5 xenoliths. Although the granite outcropping in the volcanic field does contain quartz, feldspar, biotite and accessory titanite, the multi-element pattern is significantly dissimilar to the bulk rock xenoliths. Additionally the MgO and CaO contents are much higher than the xenoliths (Fig. 5C and D). As these components would not be greatly affected by partial melting of the constituent minerals observed in the sampled granite, their low abundances are inconsistent with the sampled granite being the protolith.

The monzogranite described by Wu et al. (2012) is a potential protolith to the Huoshaoshan xenoliths, however a similar problem is encountered with regard to the MgO and CaO signatures in the xenoliths. Additionally, Wu et al. (2012) describe the monzogranite as being composed of 66% feldspar and only 20% quartz. This is inconsistent with the proportion of residual feldspar found in the xenoliths being less than the abundance of quartz. The two metamorphic supracrustal lithologies described by Wu et al. (2012) – which do not outcrop at Wudalianchi but are known to be present in the Heilongjiang area – are strong possibilities. The biotite schist and biotite–plagioclase gneiss both display fabrics defined by bands of muscovite and biotite.

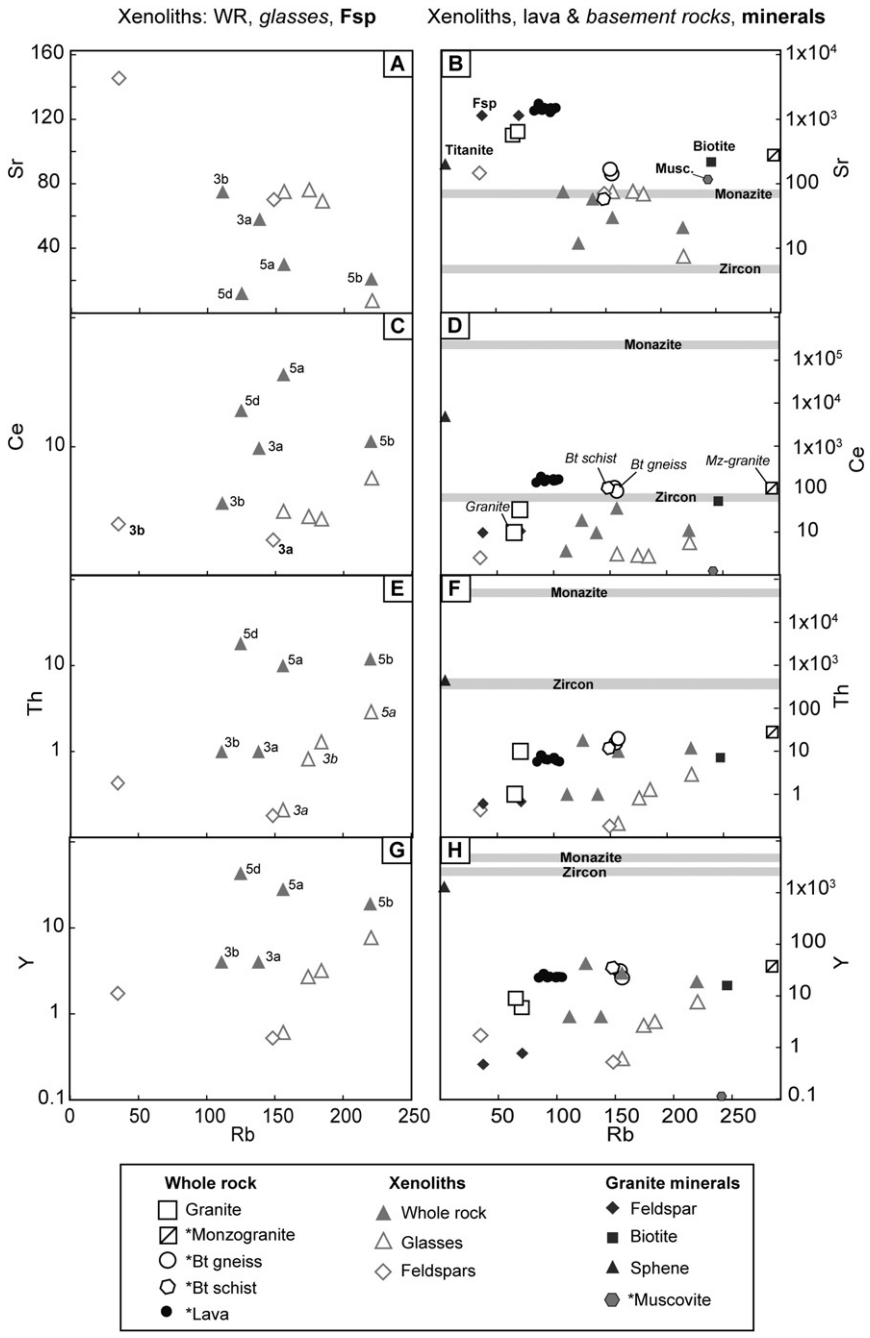

Fig. 6. Bulk rock trace element compositions of the partially melted xenoliths, their glasses and feldspars (A, C, E, G), and the Wudalianchi lava, basement rocks (as in Fig. 5). Minerals from the granite (this study) and the literature are shown in B, D, F, H. Data sources: muscovite: Ayres and Harris (1997, leucogranite); zircon: Belousova et al. (2002, granitoid) monazite: Rubatto et al. (2013, migmatite). Note that zircon and monazite are given only on the Y-axis as no Rb data were available. All data are in ppm.

They both contain accessory zircon (and apatite), feldspars and quartz. Additionally, these two lithologies display similar trace element abundances to the xenoliths (Fig. 6) and a multi-element pattern similar to the group 5 xenoliths (Fig. 7C). However, the biotite–plagioclase gneiss is described as containing only 4% quartz as opposed to 35% in the biotite schist, making the latter a more realistic option considering the amount of residual quartz observed in the xenoliths. Additionally, the biotite schist has a comparable abundance of CaO to the xenoliths (Fig. 5D).

In conclusion, from a combination of petrographic examination of the residual mineralogy combined with the bulk chemistry of the xenoliths and possible basement rock types it is likely that the partially melted crustal xenoliths at Huoshaoshan originated from a rock similar to the biotite schist described by Wu et al. (2012) containing 35% quartz, 22% feldspar, 35% biotite, 7% muscovite and accessory zircon and apatite. It is likely however, that the group 3 and group 5 xenoliths underwent different degrees of partial melting during crustal anatexis, which thus affected the residual chemistry.

6.2. The process of crustal anatexis

6.2.1. Mineralogical and chemical behaviour

The vesicular texture, presence of anatectic melts now preserved as glass, broken down minerals and high proportions of quartz observed within the crustal xenoliths allow them to be characterized as 'partially melted' and the minerals which they contain as 'residual'. Different degrees of partial melting are suggested for the different xenolith groups, based on melt and vesicle volume, residual mineral abundance and

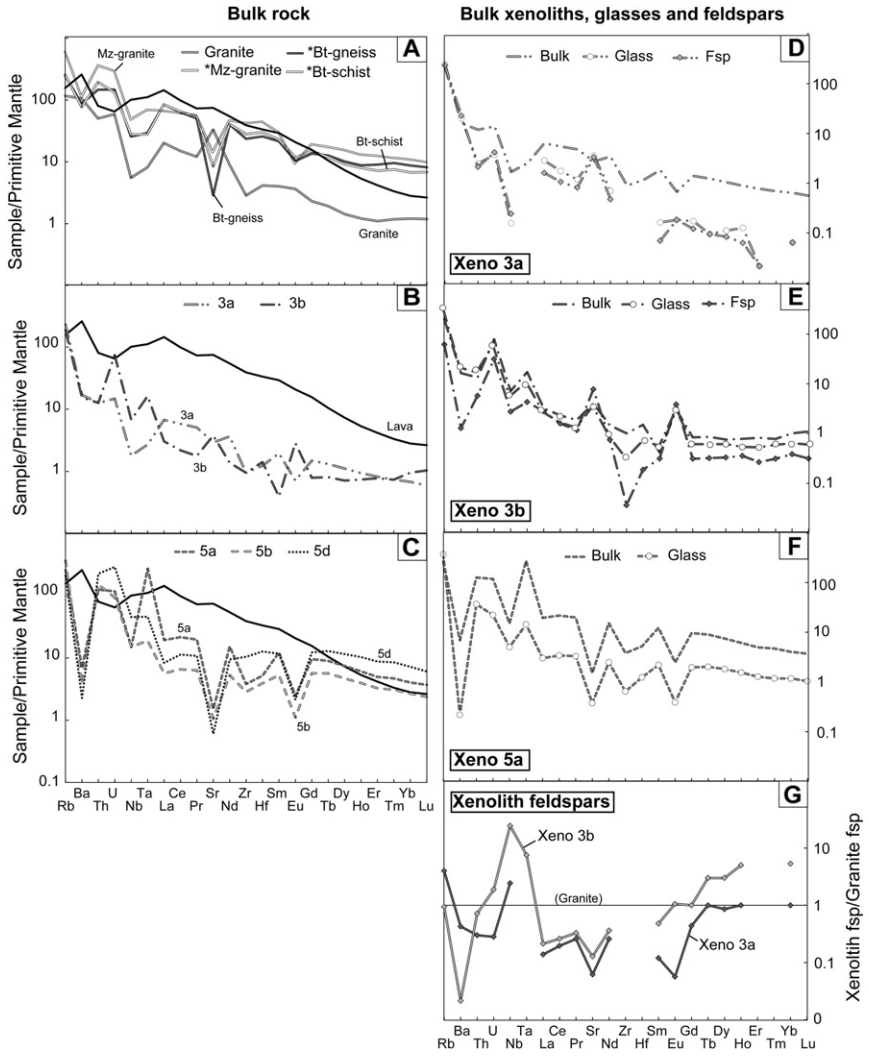

Fig. 7. Multi-element plots of bulk rock and separates for the Wudalianchi partially melted xenolith, possible protoliths and lava (this study), normalized to the primitive mantle of Sun and McDonough (1989) (A–F). A. Basement rock types (stars denote literature data) and lava (black line) from the references cited in Fig. 5. B. Bulk rock analyses of xenoliths 3a and 3b and C. 5a, 5b and 5c. D, E and F show the three xenoliths for which glass and feldspar analyses are available, compared to their bulk rock compositions (note that no feldspar was found in xenolith 5a, see Fig. 3). Interestingly, the glass chemistry follows that of the feldspars in 3a and 3b, whilst in 5a the glass composition appears to be a diluted version of the bulk rock value. In G the feldspars from 3a and 3b are plotted normally to the feldspar separated from the granite from this study, and show depletions and enrichments in certain elements (see discussion). Primitive mantle normalization values are from Sun and McDonough (1989).

type. These xenoliths appear to form a melting spectrum from samples which contain feldspar, quartz and a little biotite (xenolith 3a) to samples which contain only quartz (xenolith 5d); additionally, there is an increasing volume of anatectic melt through this series (Fig. 3), and an increase in incompatible elements (e.g. Rb) (Fig. 6) which is suggestive of higher degrees of melting affecting xenoliths 5a–d.

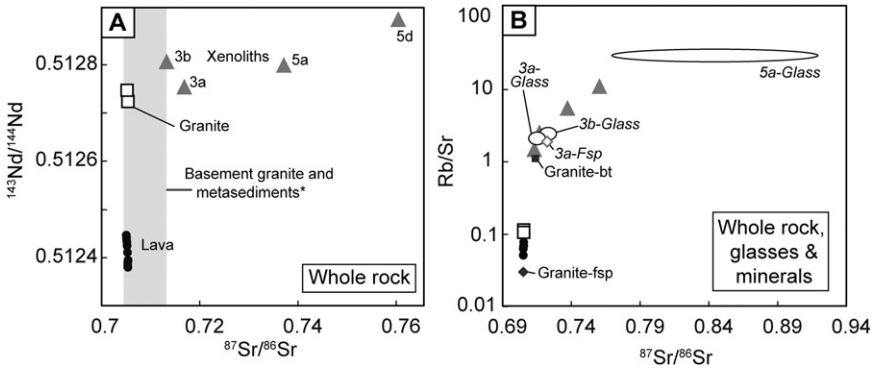

Fig. 8. A. Bulk rock $^{87}Sr/^{86}Sr$ *vs.* $^{143}Nd/^{144}Nd$ for the lava (from Zou et al., 2003), basement rock types (grey field marked with a star, data from Zhang et al., 1995, granite data from this study) and xenoliths. The latter displays a greater range in $^{87}Sr/^{86}Sr$ than the potential protoliths plotted here. B. $^{87}Sr/^{86}Sr$ *vs.* Rb/Sr of the granite mineral separates, xenolith glasses and feldspars. Glasses 3a and 3b are similar to their whole rock host values, 5a glass shows extreme disequilibrium. It is also noted that the feldspars from xenolith 3a have a much higher Rb/Sr ratio than the feldspars from the granite, due to the formers' depleted Rb compositions. See text for discussion.

Fig. 9 shows the correlation between chemical parameters of the bulk rock xenolith, the complementary glass analyses and the approximate volume of anatectic melt contained within the xenoliths (note that a higher volume of melt present in the xenolith is here interpreted as representing a greater extent of anatexis). There is a clear correlation between the volume of melt, increasing SiO_2 and decreasing Al_2O_3, which is consistent with the decrease of feldspar and biotite and the increasing abundance of quartz as a residual mineral phase through the xenolith suite from 3a to 5d. The conclusion can be drawn that the extent of control on the melt chemistry by certain mineral phases is related to the degree of partial melting that the xenolith has undergone. At low melt volumes (*c.* 20%), glasses show excesses of Ba and Sr compared to their bulk xenoliths, whereas at higher melt volume the glasses show deficits of these elements. This suggests that at lower degrees of crustal anatexis, feldspars and aluminosilicate minerals are melted first (*c.f.* Knesel and Davidson, 1996) and their constituent elements concentrated in the melt phase, and thus the melts follow the chemistry of the feldspars. At higher degrees of partial melting, anomalies in Ba, Sr and Eu are still prominent, but instead of following the pattern of the feldspars as in 3a and 3b, the glass is additionally depleted in all elements almost consistently on the scale of one order of magnitude, Fig. 7F, which suggests that almost all mineral phases of the bulk xenolith have been digested and are therefore diluted in the melt. Low melt volume glasses have similar contents of HFSEs compared to their bulk xenoliths, whilst high melt volume glass (>70%) exhibits deficits in these elements, however it must be noted that xenoliths 3a and 3b contain virtually no HFSEs, suggesting that they no longer contain accessory phases. The fact that the bulk rock group 5 xenoliths contain high levels of Y, Zr and Nb (up to 43 ppm, 110 ppm and 30 ppm respectively) indicates the retention of an accessory phase in the residuum which has not therefore entered the melt phase. The latter observation does not follow what is expected in the melting of accessory phases, where it is thought that they can be completely consumed during very small degrees of melting (Wilson, 1989); although it has been suggested in later studies that they are less soluble than the major rock-forming minerals (Acosta-Vigil et al., 2010).

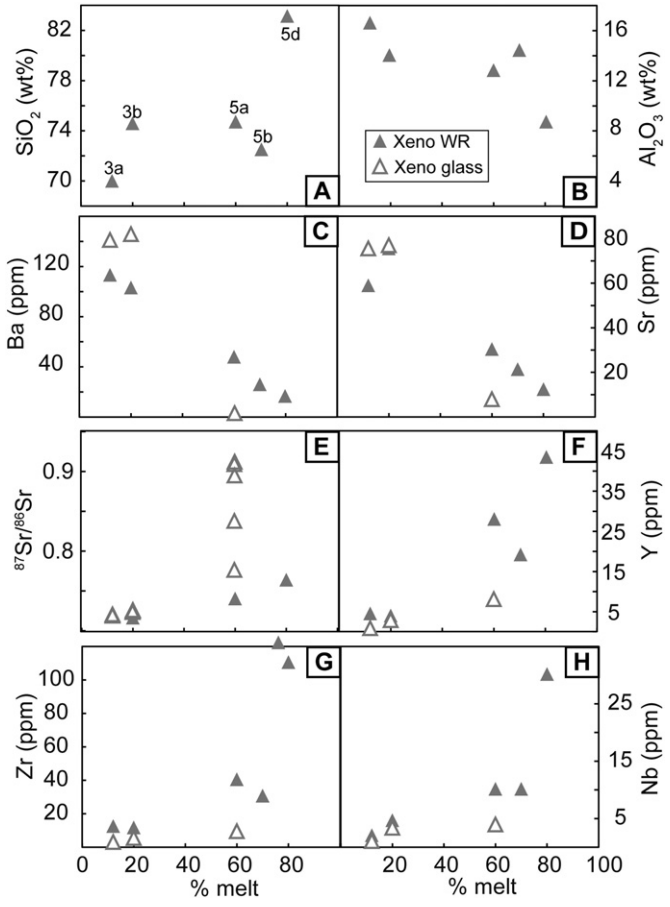

Fig. 9. Bulk xenolith and glass analyses from the xenoliths plotted against their approximate percentage of silicic melt (as reported in Fig. 3). Clear trends are observed in both major and trace elements, and $^{87}Sr/^{86}Sr$. Here, percentage of silicic melt in the xenoliths is taken as a proxy for the extent of melting of the protolith. Decreases in elements common in feldspars and micas are observed with increasing degrees of melting (B–D), whilst increases in elements common in accessory phases (F–J) with increasing degrees of melting are observed. In all cases the glass of the more melted xenolith 5a is depleted with respect to its host (except in $^{87}Sr/^{86}Sr$). Xenolith 5a is inferred to have undergone the highest degree of partial melting.

The melting out of feldspar and mica from xenoliths 3a and 5a, and the retention of an accessory phase in 5a are only particularly apparent when the glass compositions are subtracted from the whole rock xenolith values (see final column labelled 'calculated residue' in Table 2). All 'residues' display strong depletions in Rb (due to biotite removal in addition to partial melting), Ba in xenoliths 3a and 3b (most likely due to muscovite and feldspar removal), but all residues contain Zr, La and Ce. This suggests that the bulk rock xenoliths still contain an accessory phase(s) which has not entered the melt. These concentrations are higher in 5a, and the HREE is elevated also, suggesting that either it contained more of the accessory phase initially in the protolith, or that it has simply retained more than in xenoliths 3a and 3b. Compositions of minerals from the granite found outcropping close to the historic volcanoes are plotted in Fig. 6, along with muscovite and accessory minerals from the literature (see figure caption). It can be seen that all the plotted accessory phases are significantly enriched in most trace elements and would therefore have to be contained in the xenoliths or glass in extremely small amounts. Ayres and Harris (1997) documented the contribution of accessory phases to element budgets during crustal anatexis, and plotted multi-element patterns of zircon, monazite, apatite and garnet in rocks ranging from granites to metapelites. Monazite is highly enriched in all the REE (greater than 1000 times chondrite in the HREE, and up to 1,000,000 times chondrite in the LREE), which does not fit with the observed patterns in the Huoshaoshan xenoliths. Zircon has a HREE-enriched pattern, but displays a negative Eu anomaly and a peak at Ce. The retention of zircon – especially in xenolith 5a – could explain the composition of the 'residue'. This is consistent with the hypothesised protolith being the biotite-schist which contains zircon as an accessory phase. Alternatively, the presence of accessory titanite may explain the presence of Nb in the calculated 'residue', and the relatively high Y and LREE in xenoliths 3a and 3b. This was, however, not recognized as an accessory phase in the biotite-schist of Wu et al. (2012). Apatite and rutile are not considered potential accessory phases present due to the lack of similarity with their characteristic patterns: very high Nb in rutile and concave REE pattern in apatite (Meyer et al., 2011; Ayres and Harris, 1997 respectively). An attempt to reconstruct the potential protolith (biotite schist), using the bulk xenolith trace element composition, and compositions of minerals either present as residual mineral phases or deduced from the above discussion is shown in Fig. 10. The bulk xenolith was used as a starting composition, and mass balancing calculations involving feldspar, biotite, muscovite and titanite were applied. All xenoliths could be brought back to the assumed protolith with the addition of these mineral phases (Fig. 10). The addition of 0.05% zircon was found to reproduce the Zr–Hf contents of the protolith, and suggests that the pronounced negative anomaly displayed in all of the xenoliths is potentially due to melting in the presence of zircon, and subsequent removal of a part of this melt (as the glass compositions also exhibit this characteristic, Fig. 7). If the assumption of the protolith (or at least a protolith similar to the biotite schist of Wu et al. (2012)) is correct, this modelling suggests that although all xenoliths have lost a melt at some stage, xenoliths 3a and 3b have lost a greater proportion of this melt compared to xenolith 5a. This melt almost certainly was dominated by feldspar and muscovite, based on the strong depletions in Ba, Sr and Eu in xenoliths 3a and 5a, but is likely

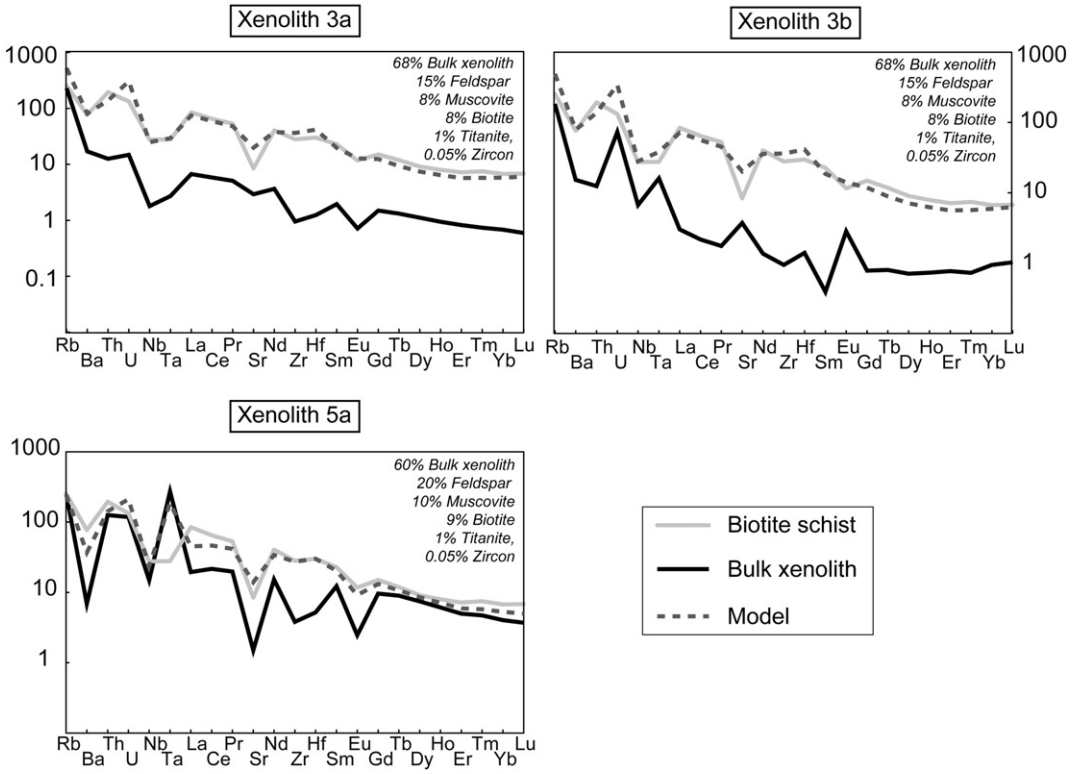

Fig. 10. Mass balance models recreating the assumed protolith (biotite schist) of the Huoshaoshan xenoliths from each bulk xenolith composition. Percentages in italics show the quantities of minerals required to achieve a good match between the biotite schist (grey line) and the model (dashed line). A good match is achieved in almost all elements, with the exception of Ta in xenolith 5a which displays a prominent positive anomaly. A notable feature is that zircon has to have been extracted to create the characteristic Zr–Hf dip in all the xenoliths. The feldspar, biotite and titanite compositions used in the model are from the granite sample of this study, and the muscovite composition is from Ayres and Harris (1997).

to have also contained zircon. The relatively high abundances of HFSEs in xenolith 5a compared to group 3 suggest the presence of a second accessory phase such as titanite which has been partially retained in the former.

Interestingly, when the feldspars contained in xenoliths 3a and 3b are normalized to the granite feldspars (Fig. 7G) there are notable differences which suggest loss and exchange of material from other phases. Enrichments in Nb (and in the HREE in 3b) in the xenolith-hosted feldspars suggest the incorporation of accessory phase elements, whereas the depletions in Sr and the LREE (and Eu in 3a) are indicative of loss of material due to partial dissolution of the feldspars. From the observation that the chemistry of bulk rock xenoliths 3a and 3b follows their (melted) feldspar chemistry, it is likely that feldspar dominates the remaining assemblage. However, this does not explain where the relatively enriched component of the residue has gone (especially in the case of xenolith 3a, Fig. 7D). Xenolith 3b, its feldspar and glass compositions are relatively similar, except for strong depletions in Ba and Zr in the feldspar (Fig. 7E), and unlike the other xenoliths, display strong positive Sr and Eu anomalies. The overall bulk chemistry of this xenolith suggests that despite being partially melted, it has retained the majority of its components.

The Sr-isotopic compositions of sampled glasses – especially that of xenolith 5a – are distinct from that of the bulk xenoliths (Fig. 8B), and indicate that disequilibrium melting has occurred during crustal anatexis (e.g. Knesel and Davidson, 1996; Grove et al., 1988). From this, the question arises of which variable Rb/Sr-bearing minerals have contributed to the composition of the anatectic melts. The Rb/Sr composition of glass 5a is significantly higher at 29.4 than the other glasses and the biotite and plagioclase feldspar from the granite which range from 2.68 to 0.033 respectively. This may reflect the contribution from a high Rb/Sr mineral phase which has been exhausted during crustal anatexis. Ruling out biotite (at least that of similar composition to the granites), muscovite is a potential phase that could produce melts with high Rb/Sr and elevated $^{87}Sr/^{86}Sr$ signatures. This phase has been documented in the biotite schist from the Heilongjiang area as described by Wu et al. (2012, see earlier section).

6.2.2. Constraints on immersion time of the xenoliths

A greater abundance of hydrous minerals, such as muscovite, has the potential to explain the greater quantity of vesicles and melt in the group 5 xenoliths. However, the greater degree of partial melting displayed by the group 5 xenoliths could also suggest that they spent more time enclosed in ascending basalt than those in group 3. Further evidence for this are the locations on Huoshaoshan: group 3 in a′a type lava in the scoria cone (the first to be erupted), and group 5 within pahoehoe lava flows which were erupted later. Eye-witness accounts documented in Feng and Whitford-Stark (1986) describe several years of eruptive activity at Huoshaoshan and Laoheishan, suggesting that if the lava flows were erupted later than the scoria cone, there may have been several years in which the group 5 lavas were enclosed in basaltic magma, although the experimental study of McLeod and Sparks (1998) modelled that continental crust lithologies may melt in magma as rapidly as 2 mm per hour, therefore the difference between groups 3 and 5 could be on the scale of weeks rather than years. This shorter timescale is more consistent with the experimental work of Edwards and Russell (1996) and Shaw (2000), who measured the change in radius of various silicate minerals at a range of temperatures and pressures. Wudalianchi magmas are thought to be produced at temperatures of 1200–1250 °C (e.g. Kuritani et al., 2013); Edwards and Russell (1996) suggest that for temperatures of 1100 °C it would take on the order of 3–4 days for a 1 cm feldspar grain to be completely dissolved, and 20 days for a 1 cm quartz grain. We assume that the Wudalianchi magmas would be somewhat cooler than this by the time crustal lithologies are encountered. As quartz persists as a residual mineral phase

throughout the xenolith suite, this places a limit on the duration of immersion (i.e. significantly less than *c.* 20 days). The fact that residual feldspar is only present in the group 3 xenoliths suggests that the difference in immersion time between group 3 and group 5 could be on the order of a few days, and this is suggested as the explanation for why the group 5 xenoliths contain only residual quartz, and a greater volume of anatectic melt compared to group 3 (Figs. 3 and 9). The study of Shaw (2009) uses the development of a melted boundary layer between xenolith and host as one way to calculate the duration of heating of xenoliths from Rockeskyllerkopf volcano, West Eifel, Germany, using the experimentally determined timescales of Shaw (2000) to calculate growth rate ($5 \times t^{0.5}$ μm/s). Using this calculation, we can estimate the time of formation for the boundary layer of xenolith 5b (*c.* 500 μm, shown in Fig. 4B) as approximately 3 h. However, this timescale presumably starts from the point at which melt is produced within the xenolith, not the time of the initial immersion and heating; we therefore hypothesise the time of immersion for the xenolith suite to be on the order of several hours up to several days.

Farina and Stevens (2011) showed that for granitic melts, the greater the duration of melting, the higher the $^{87}Sr/^{86}Sr$ of the resultant melt, and this feature is especially prominent with respect to biotite and muscovite, less so for plagioclase. This could add further evidence for the longer immersion time of the group 5 xenoliths; however, the study considered timescales on the scale of hundreds of millions of years rather than those expected for ascending basalt. Studies of the latter case have in fact observed the reverse phenomenon: initial melts are highly radiogenic (in $^{87}Sr/^{86}Sr$) and with increased degrees of melting approach the whole-rock isotopic composition (e.g. Knesel and Davidson, 1996, 1999; Tommasini and Davies, 1997). In the case of the Huoshaoshan xenoliths the opposite is observed: the xenoliths which have undergone the greater degrees of partial melting contain glass which exhibits the highest radiogenic $^{87}Sr/^{86}Sr$ signatures. We suggest that this supports our hypothesis that the group 3 xenoliths have lost the enriched portion of their melt, and the group 5 xenoliths have retained it. Due to this, and the fact that the difference between the bulk xenolith and glass chemistry cannot be accounted for by the residual minerals observed in the group 3 or 5 xenoliths, we discuss the possibility that this enriched melt has been lost from the xenoliths.

6.3. Implications for crustal contamination of basaltic magmas

There have been several natural examples described in the literature where anatexis of crustal rocks types has been shown to contaminate ascending magmas (e.g. Al-Rawi and Carmichael, 1967; Grove et al., 1988). It was first suggested by Gorai (1940) that the anomalous chemistry of the Wudalianchi lavas (high K_2O and LILE abundances) could be due to large-scale assimilation of crustal lithologies during basaltic magma ascent. Later studies of the Wudalianchi volcanic field, however, have demonstrated that bulk assimilation of crustal rock types cannot explain the enriched chemistry of the lavas, for example; 1) the high ^{230}Th-excess displayed by the lavas: $(^{230}Th/^{238}U) = 1.24–1.33$, which would otherwise be expected to be diluted by Mesozoic or Cretaceous crustal rock types in U–Th equilibrium (Zou et al., 2003), 2) the similarity of whole rock Sr–Nd isotopes between basement rock types and lavas (Zhang et al., 1995) (Fig. 8A), and 3) the fact that the potential basement rock types plotted in Figs. 5–7 generally have lower concentrations of major and trace elements than the lavas would imply that large-scale incorporation of these lithologies would result in a dilution of these components in the lavas. There is, however, a positive correlation between whole rock SiO_2 and $^{87}Sr/^{86}Sr$ in the lavas (data from Zou et al., 2003; Zhang et al., 1995) which could be interpreted as recording the influence of crustal assimilation. However, as the xenoliths in the present study were found in eruptive material from the Huoshaoshan volcanic center, which has lower SiO_2 and less radiogenic $^{87}Sr/^{86}Sr$, it is difficult to assess the relevance of this trend within the context of this study.

As detailed in Grove et al. (1988), there are three main mechanisms of crustal contamination: 1) bulk assimilation; the complete digestion of crustal material, 2) assimilation of partial melt; a part of the melt is digested into the melt, but the xenolith maintains its physical structure, and 3) selective assimilation; where only certain components are transferred between xenolith and lava. If bulk assimilation had occurred, partially melted xenoliths present would not be preserved in the Huoshaoshan lavas. Assimilation of a partial melt or selective assimilation are likely scenarios which would account for the loss of melt from the xenoliths and can be tested as potential processes through which the lavas at Huoshaoshan are contaminated.

When the Huoshaoshan lava is compared with Cenozoic, non-potassic basalts from nearby volcanic fields in NE China (Jingbohu and Long-gang, Zou et al., 2008), the former is relatively enriched in many of the elements discussed in the previous section which could have been liberated from micas and feldspars (Rb, Ba, Sr), but also some accessory-phase elements (Zr and Hf). These lavas are taken as potential 'unenriched' versions of the Huoshaoshan, with the most primitive sample of Long-gang used for modelling as it has a similar multi-element pattern to Huoshaoshan, but is less enriched and with less extreme positive Ba and La anomalies. Assimilation of a partial melt was modelled by simple mass balancing of the glass compositions of the xenoliths and the Long-gang lava. This scenario however causes a decrease in all element abundances (with the exception of Rb). Assimilation of a partial melt therefore seems an unlikely scenario. Selective assimilation from granite to basalt was experimentally modelled by Watson (1982), who found that downhill diffusion of K_2O from granite to basalt occurs independently of other elements (such as Na_2O, which remains stable) within a system. This process could be evidence for the assimilation of feldspar-rich melts being the cause of the potassic nature of the basalts, and their similarity in Na_2O contents compared to other non-potassic basalts in the area such as Jingbohu and Long-gang. It must be noted, however, that mantle source-related causes have also been attributed to the potassic nature of the basalts by several authors (Kuritani et al., 2013; Zhang et al., 1995; Zou et al., 2003). In the study by Grove et al. (1988), a composition for the selective melt was hypothesised using high-degree melts contained in lava-enclosed xenoliths and estimations made regarding gains and losses of elements to calculate a potential assimilant. In the case of the Huoshaoshan xenoliths, we show that there is a component which is not accounted for in either the residual mineralogy or the sampled glasses. An estimation can be made as to whether this residual melt could potentially cause the anomalies observed in the Huoshaoshan lava by adding a portion of the calculated 'residue' from Table 2 to the Long-gang lava composition. To take the example of the calculated residue from xenolith 5a, a decrease in most elements with the exception of Ta (which displays a large positive anomaly) is observed, and with the addition of a larger proportion of this component, an anomaly at Zr–Hf appears (on a primitive mantle normalized multi-element plot). This latter feature is not present in the Wudalianchi lavas. We therefore conclude that the missing component has not had a significant chemical effect on the enclosing lavas.

Despite the lack of strong evidence for large-scale crustal contamination, the xenoliths undoubtedly show evidence for the loss of an anatectic melt, and interaction between felsic melt and the enclosing lava is visible on the micro-scale (Fig. 4). Xenolith 3a contains complex melt pockets containing mafic and silicic melts which have incompletely mixed (Fig. 4A). This suggests that geochemical heterogeneity of anatectic melts likely exists on very local, micro-scale (*c.f.* McLeod et al., 2012). The well-preserved contact zone between xenolith and lava in xenolith 5b shows features such as olivines being pushed down between vesicles in the xenolith (Fig. 4B) and one left stranded (Fig. 4C), and silicic melt as a rim along the contact. The experimental study of Mcleod and Sparks (1998) demonstrates that partial melting produces a crystal-melt mush at the xenolith edge, such as the contact that is observed in xenolith 5b (Fig. 4B). A notable feature of this mixing zone is

that it doesn't visibly extend more than 0.5 mm into the lava and that the silicic melt has a sharp contact with the lava. This suggests that the viscosity contrast was too great for the melt to infiltrate the basaltic groundmass, whilst pyroxene microlites have been incorporated along the side of one of the vesicles, suggesting that transfer of material occurs from lava to xenolith but is less visually obvious from xenolith to lava. It may be that the viscosity difference between a′a and pahoehoe lava (the former being more viscous due to loss of gas, Macdonald, 1953) is the reason why xenolith 3a has lost more melt than xenolith 5a. We suggest that whilst disequilibrium melting has obviously occurred throughout the whole xenolith suite (in some xenoliths more extremely than others), rather than being lost to the enclosing basalt components are distributed in pockets and at the interface of the xenolith. Further, more spatially-focused studies of the micro-scale textures of partially melted xenoliths will provide additional insights as to where and how anatectic melts are distributed during crustal partial melting and constrain the geochemical budgets of open magmatic systems.

7. Summary and conclusions

- A suite of naturally occurring partially melted crustal xenoliths enclosed in basalt lava were sampled from Huoshaoshan volcano in the Wudalianchi volcanic field of NE China. All samples were analysed for their bulk rock, glass and mineral compositions in order to investigate the elemental and isotopic budgets of open magmatic systems.
- The xenoliths contain residual minerals, anatectic melt preserved as mainly silicic glass, and abundant vesicles. Analysed glasses are more depleted with respect to trace elements than their host xenoliths, which in turn are all relatively depleted with respect to potential protoliths from the area.
- The residual mineralogy and preserved textures suggest that the protolith to these partially melted crustal xenoliths was metamorphic and contained abundant quartz and feldspar, hydrous phases such as biotite and muscovite, and accessory phases in small quantities, likely zircon and titanite. Differences between the two groups of xenoliths are hypothesised as being due to varying degrees of crustal anatexis which probably occurred over the span of several days.
- Striking correlations between the volume of melt contained in the xenoliths, and the compositions of the bulk rock and glass separates are evidence that the degree of melting has a large control on the involvement of mineral phases at different stages of anatexis.
- Glasses in xenoliths 3a and 3b follow the composition of feldspars contained in the same xenoliths, suggesting that these melts are dominated by dissolution of feldspars. The glass in xenolith 5a however, whilst still being depleted with respect to its host xenolith, is more enriched than those in 3a and 3b.
- $^{87}Sr/^{86}Sr$ is higher and more variable in the xenoliths than potential protoliths, which support disequilibrium during crustal anatexis involving biotite and/or muscovite. Glass 5a displays extremely high values: if we assume that previous models (based on experimental and natural examples) of disequilibrium melting are correct and that lower degrees of melting create higher $^{87}Sr/^{86}Sr$, this suggests that a proportion of (enriched) melt has been lost from xenoliths 3a and 3b, but is retained in xenolith 5a.
- Loss of melt is supported by depletions in elements which are common in minerals not observed in the residual xenolith, such as large depletions in Ba caused by muscovite, and characteristic depletions in Zr–Hf attributed to melting in the presence of zircon.
- If the assumed protolith – biotite schist – is correct, some of the compositional features of the bulk xenoliths and glasses can be explained by loss of an enriched melt containing zircon, and some feldspar and micas which was lost from all of the xenoliths, but more extensively from 3a than in 5a. This is counter intuitive given the latter's greater extent of anatexis. We hypothesise that this is due to the viscosity difference with the lava enclosing the two groups of xenoliths.
- Micro-scale interaction is observed between the lava and the xenoliths. However, we conclude that it is not a large-scale modifying process at Wudalianchi.

Acknowledgements

We are grateful to Geoff Nowell for guidance throughout whole rock Sr–Nd and micro-Sr analysis at Durham University. We extend thanks to Chris Ottley for tuition and guidance through full procedure of rock crushing and solution ICP-MS analysis at Durham University and Nic Odling and Godfrey Fitton at the University of Edinburgh for providing major element data. Samples were collected as part of a Royal Society exchange visit, supported by funding awarded to Yaoling Niu. We benefitted from discussions during fieldwork with Yaoling Niu, Dougal Jerram, David Selby and Thor Thordarsson. We thank Editor Klaus Mezger, Silvio Ferrero and an anonymous reviewer for their constructive comments, and additionally the Durham Volcanology Group for discussion and reviews on earlier drafts of this manuscript, and for the comments of Antonio Acosta-Vigil, Tim Grove and an anonymous reviewer from a previous version of this manuscript, which greatly improved the study. The authors acknowledge their own patience and perseverance after 5 years of working on this dataset and can now be found in the pub. LEM is supported at CEGA by FONDAP (Fondo de Financiamiento de Centros de Investigación en Áreas Prioritarias) project 15090013.

References

Acosta-Vigil, A., Buick, I., Cesare, B., London, D., Morgan, G.B., 2012. The extent of equilibration between melt and residuum during regional anatexis and its implications for differentiation of the continental crust: a study of partially melted metapelitic enclaves. J. Petrol. 53 (7), 1319–1356.
Acosta-Vigil, A., et al., 2010. Mechanisms of crustal anatexis: a geochemical study of partially melted metapelitic enclaves and host dacite, SE Spain. J. Petrol. 51 (4), 785–821.
Al-Rawi, Y., Carmichael, I.S.E., 1967. A note on the natural fusion of granite. Am. Mineral. 52, 1806–1814.
Annen, C., Blundy, J.D., Sparks, R.S.J., 2006. The genesis of intermediate and silicic magmas in deep crustal hot zones. J. Petrol. 47 (3), 505–539.
Ayres, M., Harris, N., 1997. REE fractionation and Nd-isotope disequilibrium during crustal anatexis: constraints from Himalayan leucogranites. Chem. Geol. 139 (1–4), 249–269.
Belousova, E., Griffin, W., O'Reilly, S., Fisher, N., 2002. Igneous zircon: trace element composition as an indicator of source rock type. Contrib. Mineral. Petrol. 143 (5), 602–622.
Bowen, N.L., 1928. The Evolution of the Igneous Rocks. Dover Publications, New York (334 pp.).
Cesare, B., 2000. Incongruent melting of biotite to spinel in a quartz-free restite at El Joyazo (SE Spain): textures and reaction characterization. Contrib. Mineral. Petrol. 139 (3), 273–284.
Cesare, B., Salvioli-Mariani, E., Venturelli, G., 1997. Crustal anatexis and melt extraction during deformation in the restitic xenoliths at El Joyazo (SE Spain). Mineral. Mag. 61 (1), 15–27.
Charlier, B.L.A., et al., 2006. Methods for the microsampling and high-precision analysis of strontium and rubidium isotopes at single crystal scale for petrological and geochronological applications. Chem. Geol. 232 (3–4), 114–133.
de Silva, S.L., 1989. Altiplano-puna volcanic complex of the central Andes. Geology 17 (12), 1102–1106.
DePaolo, D.J., 1981. Trace element and isotopic effects of combined wallrock assimilation and fractional crystallization. Earth Planet. Sci. Lett. 53 (2), 189–202.
Edwards, B.R., Russell, J.K., 1996. A review and analysis of silicate mineral dissolution experiments in natural silicate melts. Chem. Geol. 130 (3–4), 233–245.
Farina, F., Stevens, G., 2011. Source controlled $^{87}Sr/^{86}Sr$ isotope variability in granitic magmas: the inevitable consequence of mineral-scale isotopic disequilibrium in the protolith. Lithos 122 (3–4), 189–200.
Feng, M.S., Whitford-Stark, J.L., 1986. The 1719–1721 eruptions of potassium-rich lavas at Wudalianchi, China. J. Volcanol. Geotherm. Res. 30, 131–148.
Font, L., et al., 2008. Sr and Pb isotope micro-analysis of plagioclase crystals from Skye lavas: an insight into open-system processes in a flood basalt province. J. Petrol. 49 (8), 1449–1471.
Gorai, M., 1940. A consideration of the genesis of alkali basalts from Wu-ta-lien-chih volcano, North Manchuria. J. Geol. Soc. Jpn. 47, 457–467.
Grove, T.L., Kinzler, R.J., Baker, M.B., Donnelly-Nolan, J.M., Lesher, C.E., 1988. Assimilation of granite by basaltic magma at burnt lava flow, Medicine Lake Volcano, northern California: decoupling of heat and mass transfer. Contrib. Mineral. Petrol. 99 (3), 320–343.
Hildreth, W., Moorbath, S., 1988. Crustal contributions to arc magmatism in the Andes of central Chile. Contrib. Mineral. Petrol. 98 (4), 455–489.

Hogan, J.P., Sinha, A.K., 1991. The effect of accessory minerals on the redistribution of lead isotopes during crustal anatexis: a model. Geochim. Cosmochim. Acta 55 (1), 335–348.
Hsu, C., Chen, J., 1998. Geochemistry of late Cenozoic basalts from Wudalianchi and Jingpohu areas, Heilongjiang province, northeast China. J. Asian Earth Sci. 16 (4), 385–405.
Kay, S.M., Coira, B.L., Caffe, P.J., Chen, C.-H., 2010. Regional chemical diversity, crustal and mantle sources and evolution of central Andean Puna plateau ignimbrites. J. Volcanol. Geotherm. Res. 198 (1–2), 81–111.
Knesel, K.M., Davidson, J.P., 1996. Isotopic disequilibrium during melting of granite and implications for crustal contamination of magmas. Geology 24 (3), 243–246.
Knesel, K.M., Davidson, J.P., 1999. Sr isotope systematics during melt generation by intrusion of basalt into continental crust. Contrib. Mineral. Petrol. 136 (3), 285–295.
Kuritani, T., Kimura, J.-I., Ohtani, E., Miyamoto, H., Furuyama, K., 2013. Transition zone origin of potassic basalts from Wudalianchi volcano, northeast China. Lithos 156–159, 1–12.
Kuritani, T., Ohtani, E., Kimura, J.-I., 2011. Intensive hydration of the mantle transition zone beneath China caused by ancient slab stagnation. Nat. Geosci. 4 (10), 713–716.
Le Maitre, R.W., 2002. Igneous Rocks — A Classification and Glossary of Terms. Cambridge University Press, Cambridge (236 pp.).
Macdonald, G.A., 1953. Pahoehoe, aa, and block lava. Am. J. Sci. 251 (3), 169–191.
McLeod, P., Sparks, R.S.J., 1998. The dynamics of xenolith assimilation. Contrib. Mineral. Petrol. 132 (1), 21–33.
McLeod, C.L., Davidson, J.P., Nowell, G.M., de Silva, S.L., 2012. Disequilibrium melting during crustal anatexis and implications for modeling open magmatic systems. Geology 40 (5), 435–438.
Meyer, M., John, T., Brandt, S., Klemd, R., 2011. Trace element composition of rutile and the application of Zr-in-rutile thermometry to UHT metamorphism (Epupa Complex, NW Namibia). Lithos 126 (3–4), 388–401.
Nowell, G.M., Parrish, R.R., 2001. Simultaneous acquisition of isotope compositions and parent/daughter ratios by non-isotope dilution solution-mode plasma ionisation multi-collector mass spectrometry (PIMMS). Plasma Source Mass Spectrometry — The New Millennium. Royal Society of Chemistry, Cambridge, pp. 298–310.
Nowell, G.M., Pearson, D.G., Ottley, C.J., Schweiters, J., Dowall, D., 2003. Long-term performance characteristics of a plasma ionisation multi-collector mass spectrometer (PIMMS): the ThermoFinnigan Neptune. Plasma Source Mass Spectrometry: Applications and Emerging Technologies. Royal Society of Chemistry, Cambridge, pp. 307–320.
Ottley, C.J., Pearson, D.G., Irvine, G.J., 2003. A routine procedure for the analysis of REE and other trace elements in geological samples by ICP-MS. Plasma Source Mass Spectrometry: Applications and Emerging Technologies, pp. 221–230.
Pearson, D., Nowell, G., 2005. Accuracy and precision in plasma ionisation multi-collector mass spectrometry: constraints from neodymium and hafnium isotope measurements. Spec. Publ. R. Soc. Chem. 301, 284.
Rubatto, D., Chakraborty, S., Dasgupta, S., 2013. Timescales of crustal melting in the higher Himalayan crystallines (Sikkim, eastern Himalaya) inferred from trace element-constrained monazite and zircon chronology. Contrib. Mineral. Petrol. 165 (2), 349–372.
Russell, J.K., Hauksdóttir, S., 2001. Estimates of crustal assimilation in Quaternary lavas from the Northern Cordillera, British Columbia. Can. Mineral. 39 (2), 275–297.
Shaw, C.S.J., 2000. The effect of experiment geometry on the mechanism and rate of dissolution of quartz in basanite at 0.5GPa and 1350oC. Contrib. Mineral. Petrol. 139, 509–525.
Shaw, C.S.J., 2009. Caught in the act — the first few hours of xenolith assimilation preserved in lavas of the Rockeskyllerkopf volcano, West Eifel, Germany. Lithos 112 (3–4), 511–523.
Spera, F.J., Bohrson, W.A., 2001. Energy-constrained open-system magmatic processes I: general model and energy-constrained assimilation and fractional crystallization (EC–AFC) formulation. J. Petrol. 42 (5), 999–1018.
Sun, S.-s., McDonough, W.F., 1989. Chemical and isotopic systematics of oceanic basalts: implications for mantle composition and processes. Geol. Soc. Lond. Spec. Publ. 42 (1), 313–345.
Taylor, J.H.P., 1980. The effects of assimilation of country rocks by magmas on $^{18}O/^{16}O$ and $^{87}Sr/^{86}Sr$ systematics in igneous rocks. Earth Planet. Sci. Lett. 47 (2), 243–254.
Thirlwall, M.F., 1991. Long-term reproducibility of multicollector Sr and Nd isotope ratio analysis. Chem. Geol. Isot. Geosci. Sect. 94 (2), 85–104.
Tommasini, S., Davies, G.R., 1997. Isotope disequilibrium during anatexis: a case study of contact melting, Sierra Nevada, California. Earth Planet. Sci. Lett. 148 (1–2), 273–285.
Waight, T.E., Lesher, C.E., 2010. Pb isotopes during crustal melting and magma mingling — a cautionary tale from the Miki Fjord macrodike, central east Greenland. Lithos 118 (1–2), 191–201.
Wang, Y., Chen, H., 2005. Tectonic controls on the Pleistocene–Holocene Wudalianchi volcanic field (northeastern China). J. Asian Earth Sci. 24 (4), 419–431.
Watson, E.B., 1982. Basalt contamination by continental crust: some experiments and models. Contrib. Mineral. Petrol. 80 (1), 73–87.
Wilde, S.A., Zhou, X., Nemchin, A.A., Sun, M., 2003. Mesozoic crust–mantle interaction beneath the north China craton: a consequence of the dispersal of Gondwanaland and accretion of Asia. Geology 31 (9), 817–820.
Wilson, B.M., 1989. Igneous Petrogenesis: A Global Tectonic Approach. Springer Science & Business Media (466 pp.).
Wu, G., Chen, Y., Chen, Y., Zeng, Q., 2012. Zircon U–Pb ages of the metamorphic supracrustal rocks of the Xinghuadukou Group and granitic complexes in the Argun massif of the northern Great Hinggan Range, NE China, and their tectonic implications. J. Asian Earth Sci. 49, 214–233.
Xiao, L., Wang, C., 2009. Geologic features of Wudalianchi volcanic field, northeastern China: implications for Martian volcanology. Planet. Space Sci. 57 (5–6), 685–698.
Zhang, M., Suddaby, P., Thompson, R.N., Thirlwall, M.F., Menzies, M.A., 1995. Potassic volcanic rocks in NE China: geochemical constraints on mantle source and magma genesis. J. Petrol. 36 (5), 1275–1303.
Zou, H., Fan, Q., Yao, Y., 2008. U–Th systematics of dispersed young volcanoes in NE China: asthenosphere upwelling caused by piling up and upward thickening of stagnant Pacific slab. Chem. Geol. 255 (1–2), 134–142.
Zou, H., et al., 2003. Constraints on the origin of historic potassic basalts from northeast China by U–Th disequilibrium data. Chem. Geol. 200, 189–201.